Origin of Sulfides in the Contact Granodiorites

of the South Mountain Batholith,

Nova Scotia

Hugh R. Samson

Department of Earth Sciences
Dalhousie University, Halifax, Nova Scotia
April 28, 2005

TABLE OF CONTENTS

TABLE OF FIGURES

CHAPTER 1

CHAPTER 2

CHAPTER 3

CHAPTER 4

TABLE OF TABLES

Acknowledgments

Abstract

Late in the Acadian Orogeny in southwestern Nova Scotia, the late Devonian South Mountain Batholith (SMB) intruded the Cambro-Ordovician meta-sandstones and siltstones of the Meguma Terrane. Whole-rock and mineral chemical data for major elements (A/CNK) and radiogenic isotopes (Sr-Nd) show that the SMB evolved by a combination of assimilation of the Meguma country rock and fractional crystallization of its magmas (AFC processes). The purpose of this investigation is to test the AFC model using textural and compositional variations in sulfide minerals from Meguma, xenolith, and SMB rock samples. The dominant sulfide phases in the Meguma, xenoliths, and SMB are pyrite and pyrrhotite, with common occurrences of chalcopyrite, and rare occurrences of sphalerite and galena. Meguma rocks distal from the contact with the SMB are dominated by anhedral, 0.25-0.5 mm pyrrhotite grains. Anhedral, 0.25-1.0 mm pyrite grains occur commonly and anhedral, <0.25 mm chalcopyrite grains occur rarely as inclusions in pyrite and pyrrhotite. Meguma samples proximal to the SMB contact contain large, 0.5-5.0 mm anhedral grains of pyrrhotite as the dominant phase, with small- to medium-sized, 0.25-1.0 mm, <0.25-1.0 mm subhedral pyrite and <0.25 mm, anhedral chalcopyrite grains occurring as inclusions in pyrrhotite. Sulfides from xenoliths near the contact of the SMB are transitional in texture and composition. Pyrrhotite is the dominant phase, occurring in large sulfide bands up to 75 mm in length, and 15 mm in width. Common inclusions of anhedral, 0.5-5.0 mm pyrite grains, and 0.25-0.5 mm chalcopyrite grains occur within xenolith samples. The SMB granodiorites contain sulfide globules exhibiting a bleb texture, which are dominated by 0.25-5.0 mm, euhedral to anhedral pyrite grains. Subhedral to anhedral, 0.25-1.5 mm chalcopyrites commonly coexist with pyrite. Distinct changes in the abundance, size, shape, and inter-granular relationships exist in the sulfide minerals from the Meguma country-rock, across the contact in xenoliths, and into the SMB. Chemical compositions of the sulfide minerals show trace amounts of As, Cu, Pb, Zn, and Ni. In SMB samples, the chalcophile trace elements Cu and Ni are preferentially concentrated in pyrite and pyrrhotite. Many of the sulfides in the SMB that occur within xenolithic remnants appear to be texturally and chemically modified equivalents of the Meguma sulfides. The concentration of chalcophile trace elements in SMB sulfide samples, as well as bleb texture associated with SMB sulfides suggest the presence of an immiscible sulfide liquid in the SMB. Models proposed for the origin of sulfides in the SMB include: primary magmatic crystallization from the silicate magma; xenocrystic from the Meguma; initially dissolved from the Meguma, then followed by crystallization from the SMB magma; and formation of immiscible droplets of Meguma sulfides that crystallized as the SMB silicate magma cooled. The latter model, involving formation of an immiscible sulphide liquid, can account for most of the textural and chemical observations, but is difficult to reconcile with known phase relations in the Cu-Fe-S system.

CHAPTER 1: INTRODUCTION

1.1 Geological History of the Meguma Supergroup

The Meguma Supergroup outcrops over an area of 32,000 km^2 over southern

Nova Scotia, as well as the same area offshore (Harris and Schenk, 1975). The Lower

Paleozoic Meguma Supergroup strata consist of inter-bedded sandstones and siltstones of

the Goldenville and Halifax Formations. The Middle to Upper Cambrian Goldenville

Formation overlies a basal unconformity. Thick-bedded sandstones, separated by thin

layers of darkly colored, sandy to silty slates, characterize this formation. The greatest

measured thickness of the Goldenville Formation is 5600 m (Fairbault, 1914). The Lower

Ordovician Halifax Formation consists mainly of siltstone and slate, with minor

sandstone beds. The thickness of the unit ranges from 4400 m in the northwest to 500 m

in the south (Taylor, 1966). The total thickness of the Meguma Group is some 10 km

(Clarke and Halliday, 1980).

Sediments forming the strata of the Meguma Supergroup indicate a deep-sea

depositional environment. Phinney (1961) concluded that the Meguma Supergroup is a

turbidite succession. Phinney's conclusions were supported and refined by many others,

including Harris and Schenk (1975), who documented strong similarities in the

Goldenville and Halifax Formation lithologies to the present abyssal plain turbidites of

the western North Atlantic (Harris and Schenk, 1975).

The source area of the Meguma sediments may be of continental origin. Harris

and Schenk (1975) hypothesized that the Meguma rocks were initially deposited off the

1

coast of northwestern Africa. Subsequent closure of the Rheic-Theic Ocean brought these strata to their current location in Nova Scotia.

Influence from the Acadian Orogeny has greatly changed the present day form of the Meguma Supergroup. The Meguma strata were folded during this Devonian orogeny, as well as metamorphosed to greenschist to amphibolite facies on a regional scale, with higher grade metamorphism around contacts with igneous intrusions (Schenk, 1973).

1.2 Geological History of the South Mountain Batholith

The South Mountain Batholith (SMB) is a large igneous intrusion that outcrops over an area of 7300 km^2 over southwestern Nova Scotia (Fig. 1.1). Emplacement of the ca. 380 Ma batholith occurred in the Meguma Terrane and was associated with the Devonian Acadian orogeny. Pre- and syn- emplacement NW- and NE- trending structural features played a significant role in the emplacement of the SMB. However, the SMB post-dates most of regional deformation of the Meguma country-rocks (MacDonald *et al.*, 1992).

MacDonald (1992) identified 13 separate plutons within the SMB. Each of these plutons is of peraluminous composition and belongs to one of two stages of plutons. Stage 1 plutons consist of biotite granodiorite and biotite monzongranite. These plutons were intruded by Stage 2 plutons consisting of leucomonzogranite and leucogranite (MacDonald *et. al,* 1992). An overall lack of deformation of country rocks, combined with prevelant metasedimentary xenoliths throughout the intrusion,

2
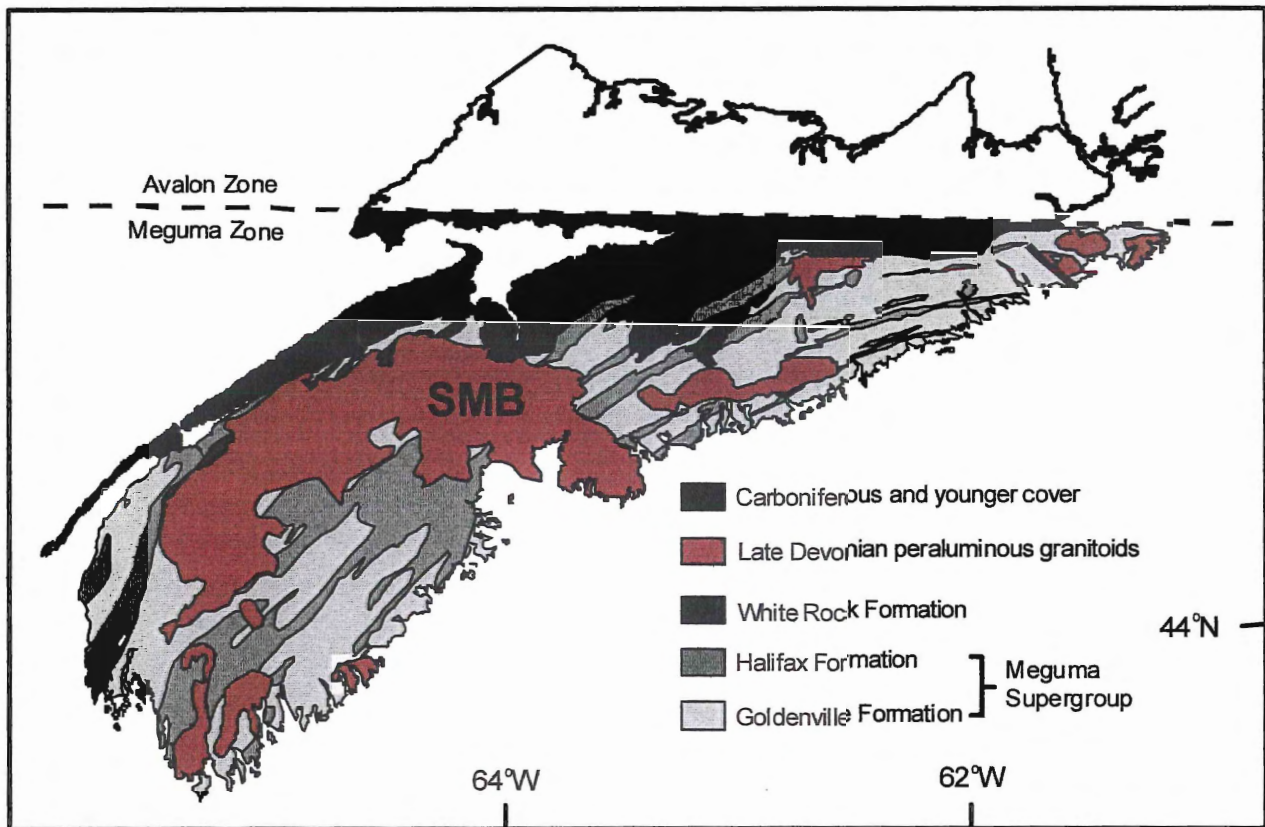
Figure 1.1 Emplacement of SMB in Meguma Supergroup, southwestern Nova Scotia

suggests that stoping was the main emplacement mechanism for the SMB at the present

level of exposure (Clarke and Muecke, 1985). Localized structures, such as primary flow

features, NW- and NE- trending faults and folds, and foliations, indicate areas of

deformation, which may suggest localized forceful emplacement (MacDonald *et. al.,*

1992).

1.3 Sulfur in the Meguma Supergroup and South Mountain Batholith

Sulfur is a volatile element that can exist in a number of different oxidation states,

each exhibiting different physical and chemical properties. The volatile nature of sulfur

leaves it more susceptible to mobilization by hydrothermal and dissolution processed

than other common elements. In magmas, sulfur readily forms immiscible sulphide

liquids if the amount of sulfur exceeds S solubility in the magma, and if T > sulfide solidus. As a result, sulfur is sensitive to interactions between magma and country rocks and, thus, it can be a valuable tool in interpreting country rock/magma relationships.

The metasedimentary rocks and greywackes of the Meguma Supergroup are rich in sulfide minerals. Average sulfur contents of the Goldenville and Halifax Formations are similar, the former being 370 ppm and the latter being 350 ppm (Poulson *et al.*, 1990). The dominant phases in these rocks are pyrite and pyrrhotite, with subordinate phases including chalcopyrite, marcasite, arsenopyrite, sphalerite, and galena (Fox *et al.*, 1997; Poulson *et al.*, 1990). Graves and Zentilli (1988) noted that further enrichment of metals occur in the Goldenville Halifax Transition Zone (GHTZ) compared with average crustal values (Fig. 1.2).

These high concentrations of metals are generally associated with sulfide minerals (Fox *et al.*, 1997). Although no studies have been done to determine sulfide mineral abundances in the GHTZ, it is important to note the sulfur enrichment in this zone.

Phase relationships of sulfide minerals in the SMB are important to describe temperature and pressure conditions during the crystallization of the batholith. Pyrite and pyrrhotite are the dominant sulfide phases in the SMB and they form anhedral to euhedral grains, which commonly occur interstitially to quartz and feldspar (Poulson *et al.*, 1990). Although some pyrite may be of secondary, hydrothermal origin, pyrite also occurs as a primary mineral in the SMB. Because pyrite can become stable in a magma only below ~750 °C, the occurrence of primary pyrite puts temperature and pressure constraints for the intrusion of the SMB at greater than 1 kbar and 650 to 750 °C, respectively
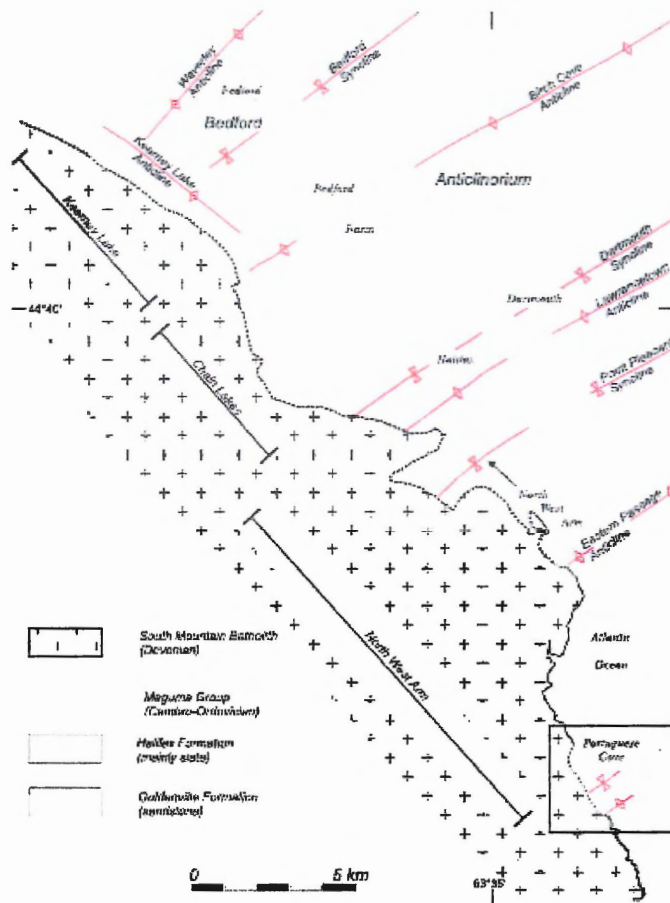
Figure 1.2 Geological map of Halifax region, illustrating Goldenville and Halifax

Formations (Culshaw and Bhatnagar, 2001)

(Poulson *et al.*, 1990). Pyrrhotite occurs in large, anhedral grains of both primary and

secondary igneous origin, but is generally less abundant than pyrite. Finally, chalcopyrite

occurs in lesser amounts the SMB. As it is stable only below 557 °C (Poulson *et. al.*,

1990), chalcopyrite is likely formed at lower temperatures either by: i) crystallization

from the magma, or ii) exsolution from pyrite and/or pyrrhotite (Poulson *et al.*, 1990).

Hydrothermal circulation during the cooling of the SMB may have enriched localized

areas of the batholith in pyrite, pyrrhotite, and other sulfide minerals.

5

1.4 Differentiation and Contamination of the South Mountain Batholith

Many studies have addressed the current geochemical and isotopic relationships in the South Mountain Batholith. There is an argument for closed-system differentiation of SMB magmas. Clarke and Halliday (1980) used Rb-Sr dates and initial Sr isotope ratios to conclude that fractional crystallization of granodiorite magma played an important role in the derivation of late intrusive stages of the batholith. Smyth and Kontak (1988) also proposed that fractional crystallization played a role in the derivation of late intrusive stages of the batholith. On the other hand, the abundance of country rock xenoliths throughout the SMB, as well examination of Sm-Nd ratios by Clarke *et al.* (1988), demonstrates an open-system contamination of the magma by the Meguma country-rock (Clarke *et. al.,* 2004).

As a result, the SMB has undergone a combination of assimilation of the Meguma country rock and fractional crystallization of its magmas, known as assimilation-fractional crystallization (AFC) (Clarke *et al.,* 1988). Late-stage fluid phases have also likely played a role in the differentiation of the SMB.

1.5 Scope and Purpose

This thesis examines sulfide minerals in the South Mountain Batholith and Meguma Supergroup with the following objectives:

1. Determine and describe changes in texture in sulfide minerals from the Meguma, to xenoliths, and finally into the SMB.

2. Determine and describe changes in composition in sulfide minerals from the Meguma, to xenoliths, and into the SMB.

6

3. Understand the processes that occurred during the emplacement of the SMB, and the sequence in which they took place to establish a model for the origin of sulfide minerals in the SMB.

1.6 Claim

In contrast to Poulson *et. al.,*(1990), who suggested that sulfides in the SMB underwent complete dissolution and recrystallization, I believe that sulfide minerals in the SMB formed as the result of partial melting of xenolith sulfides that formed immiscible sulfide melts. These migrated into the SMB, where they were subject to partial dissolution and re-crystallization during cooling of the magma.

1.7 Organizational Plan

Chapter 2 describes the methods of the investigation of sulfide minerals, beginning with the field collection of samples, followed by laboratory analysis using the electron microprobe and reflected light microscopy. Chapter 3 is a summary of the results from both field and laboratory analysis. Chapter 4 presents the implications of these results and raises arguments as to the role of sulfide minerals in the SMB and Meguma. Chapter 5 is a summary of the conclusions from this investigation.

CHAPTER 2: METHODS

2.1 Introduction

This thesis contains information about the textural and compositional characteristics of sulfide minerals occurring in the Meguma Supergroup, in Meguma xenoliths in the SMB, and in the SMB. This chapter describes the methods used to aquire the data.

2.2 Sample Collection

The first step in this investigation was to collect sulfide-bearing rock samples. Sulfide minerals occur in both the South Mountain Batholith and in the Meguma Supergroup. As one of the main points of this thesis is to determine the effect that an igneous intrusion has on sulfide minerals, the sampling strategy involved obtaining samples from the Meguma country rock, xenoliths, and the SMB. A further important consideration was to take samples from a wide variety of locations to help distinguish possible local and regional trends in sulfide texture and composition.

As a method of organization, sampling began in Meguma outcrops, in areas far enough away from the SMB to be unaffected by the intrusion. Samples were taken progressively closer to the contact of the SMB and the Meguma, and finally across the contact and into the batholith. Figure 2.1 shows the sampling locations. Sample locations in the Meguma Supergroup were chosen along the contact between the Halifax and Goldenville formations because these rocks are enriched in sulfide minerals. The rocks in this zone, known as the Goldenville-Halifax Transition Zone (GHTZ), have a rusty colour that is indicative of oxidation of sulfide minerals. Xenolith samples were collected
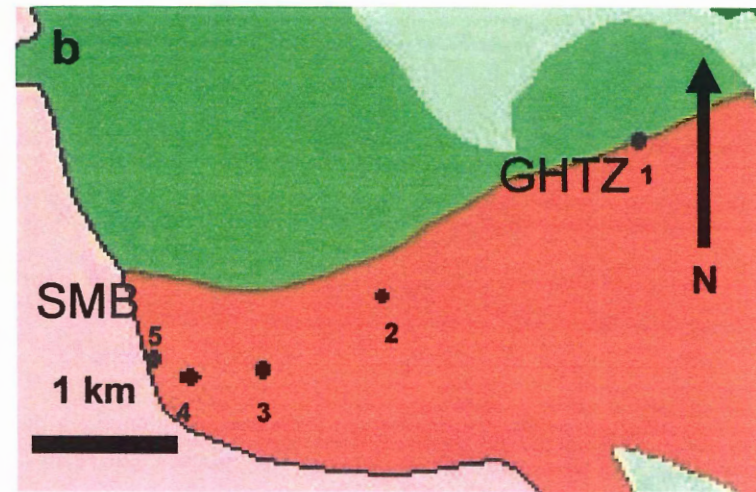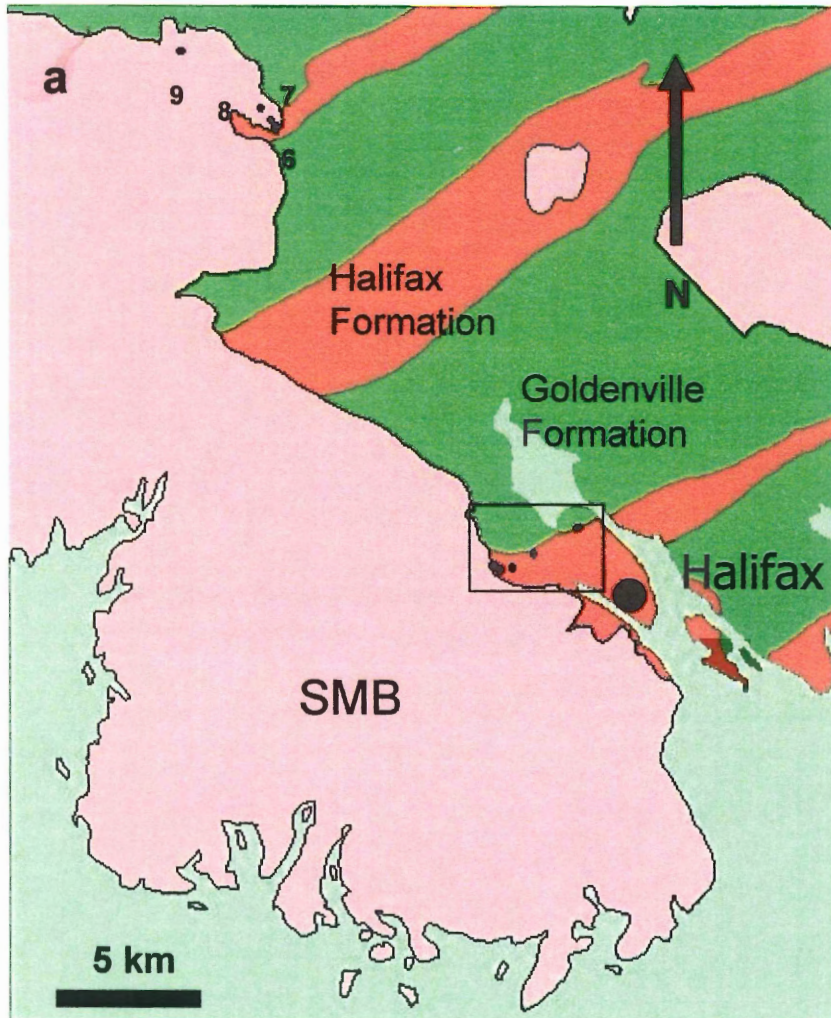
Figure 2.1 Geological Map of HRM
Sampling locations in SMB (a), and along GHTZ (b)

9

in the SMB in locations proximal and remote to the igneous contact. Appendix B documents exact sample co-ordinates.

2.3 Petrographic Analysis

Because sulfide minerals are optically opaque, phase and textural relationships are only visible using polished thin sections under reflected light. This type of observation had three main goals: i) identification of sulfides based on their high reflectivity and colour in reflected light; ii) determination of textural relationships between the sulfide minerals and the silicates; and iii) non-parallel determination of the textural relationships among sulfide minerals themselves.

2.4 Electron Microprobe (EMP) Analysis

Polished thin sections of the rock samples were further analyzed using the electron microprobe at Dalhousie University. The electron microprobe was used to determine chemical compositions of the sulfide minerals, as well as to collect electron backscatter images of the samples for analysis of texture. The elemental concentrations obtained facilitated the investigation of compositional changes occurring in sulfides, with regards to spatial relation to the contact of the SMB.

Sample preparation began with the production of polished thin sections, as in the case of optical petrology. The next step is to coat the sample with a conductive material, in this case carbon, so that electrons that strike the mineral sample are conducted away (Nesse, 2000). This coating is essential to produce a clear image of the rock sample, but it must also be thin enough (20 nm) so as to not hinder identification.

The EMP produces an image by using an internally generated electron beam, rather than by using light. Figure 2.2 shows the major components of an EMP system. A heated tungsten filament produces electrons. A voltage of 15 kV accelerates the electrons through the column where it they are focused through a series of electromagnetic lenses.
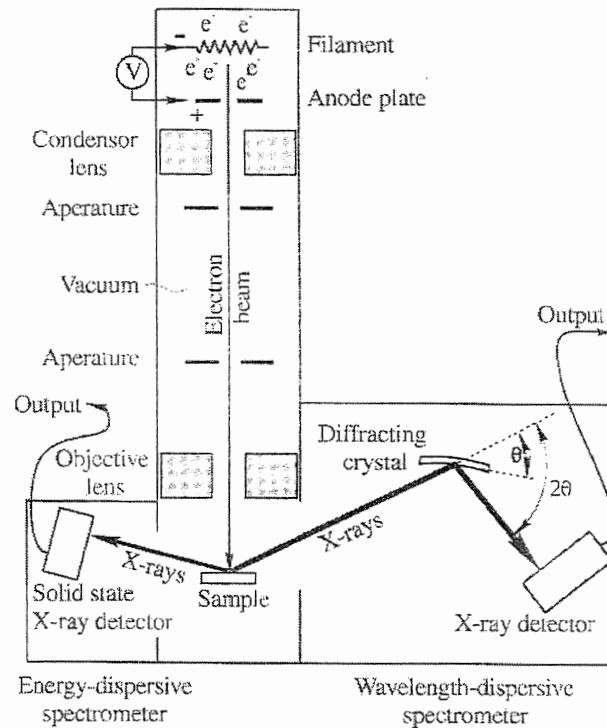
Figure 2.2 Major components of EMP system
(Nesse, 2000)

The interaction of the electron beam with the sample produces various forms of radiation, the three most important being backscattered electrons, secondary electrons, and X-rays. Each element in the sample emits a characteristic spectrum of energy, the intensity of which is proportional to its abundance in the sample. These energy spectra are recorded by the spectrometers, of which there are two types: i) an energy sensitive detector in an energy dispersive system (EDX); or ii) a wavelength dispersive system (WDX), which disperses X-rays according to wavelength. In both of these methods, the

11

instrumental response caused by the emission of characteristic X-rays is calibrated using minerals of known composition. The response, as well as the abundance of X-rays, is proportional to the concentration of each element in the sample, thus allowing the EMP to determine the chemical composition of the mineral.

For this thesis, I used the Dalhousie Regional Electron Microprobe Laboratory in the Department of Earth Sciences, Dalhousie University. The EMP in this laboratory is equipped with a JEOL JXA-8200, containing five wavelength dispersive spectrometers. The results of my analysis were achieved though the use of the WDX. The specifications were as follows: the beam current was 2×10^{-8} A, the accelerating voltage was 15 kV, counting times were 20 sec on the peak and 10 sec on each background, and the data reduction utilised ZAF matrix corrections. Table 2.1 gives the geological standards used.

Standard Mineral	Chemical Formula	Element(s) Identified
Pyrrhotite	$(Fe_{1-x}S)$	Fe, S
Arsenopyrite	$(FeAsS)$	As
Cobaltite	$(CoAsS)$	Ni
Chalcopyrite	$(CuFeS_2)$	Cu
Galena	(PbS)	Pb
Sphalerite	(ZnS)	Zn

Table 2.1 Geological mineral standards for specific element identification in EMP analysis

Element	Crystal	Spectrometer Position (mm)	Background (+) (mm)	Background (-) (mm)
S	PETJ	172.096	5.000	5.000
Fe	LIF	134.624	5.000	5.000
As	TAPH	105.131	5.000	5.000
Ni	LIFH	115.373	5.000	5.000
Pb	PETJ	169.307	5.000	5.000
Cu	LIF	107.213	5.000	5.000
Zn	LIFH	99.884	5.000	5.000

Table 2.2 Spectrometer positions for each element, as well as the dispersing crystals

Backscattered electron images of the mineral samples were produced from the EMP from electrons reflecting off the sample. The SEI image shows the texture and topography of the sample, and the BSE image shows compositional differences, used to distinguish between phases. Minerals having a higher average atomic number appear brighter in the backscatter images; conversely, minerals with a lower atomic number are darker.

2.5 Summary

Samples for this thesis were collected on the basis of their spatial relationship to the contact of the South Mountain Batholith and Meguma Supergroup. Polished thin sections of the samples were prepared in order to investigate textural and compositional relationships of the sulfide minerals. Reflected light microscopy aided in the determination of sulfide phases and textures, whereas the electron microprobe provided chemical composition of the samples.

CHAPTER 3: RESULTS

3.1 Introduction

The textures and compositions of minerals contain important information regarding their origin and any subsequent recrystallization. Samples of sulfide minerals from within the Meguma Supergroup, at the contact between the Meguma and SMB, and from locations in the SMB show variations in their textures and compositions. This chapter presents the results of the textural and chemical investigation of these samples, with a focus on pyrite, pyrrhotite, and chalcopyrite.

3.2 Textural Observations

Reflected light microscopy is necessary to examine the textures of sulfide minerals because they are opaque in transmitted light. Higher magnification study of the samples, as well as high-resolution photography, required the use of the electron microprobe. Table 3.1 summarizes mineralogical proportions, grain sizes, and other textural features of the sulfide minerals.

3.2.1 Textural features of sulfides in the Meguma Supergroup

Pyrite occurs throughout the Meguma in several different shapes and forms, ranging from subhedral to anhedral. The grains range in size from <0.25-5.0 mm and they occur as inclusions inside pyrrhotite grains, inter-grown with pyrrhotite, and as isolated grains with pyrrhotite and chalcopyrite inclusions. In the Meguma samples, pyrite commonly exists as irregularly shaped, anhedral grains (Fig. 3.1a). Remote from the contact with the SMB, pyrite is fine-grained and is relatively less abundant. Closer to

Slide	%Py	Py Grain Size(mm)	%Po	Po Grain Size(mm)	%Cpy	Cpy Grain Size(mm)	%Other	Other Grain Size(mm)	Rock Unit	Proximity to Contact
04-B	30	<0.25-1	68	0.25-5	2	<0.25	0	0	Meguma	near
04-D	5	<0.25	75	0.25-0.5	20	<0.25	0	0	Meguma	near
05-D	3	<0.25-0.25	95	3.0-5	2	<0.25	0	0	Meguma	near
05-I	18	0.5-3	75	<0.25-0.5	2	<0.25	PbS-5	<0.25-0.25	Meguma	near
07-B	0	0	98	2.0-5	1	<0.25	FeAsS-1	<0.25	Meguma	far
07-C	5	<0.25	90	0.25-5	5	<0.25	0	0	Meguma	far
07-G	1	<0.25	98	0.25-5	1	<0.25	0	0	Meguma	far
07-N	1	<0.25	95	1.0-5	4	<0.25	0	0	Meguma	far
08-D	95	0.25-0.5	5	<0.25	0	0	0	0	Meguma	far
08-F	100	0.25-0.5	0	0	0	0	0	0	Meguma	far
06-B	40	2.0-4	55	0.5-3	5	<0.25	0	0	Meguma	contact
06-D	80	2.0-5	18	0.25-0.5	2	<0.25	0	0	Meguma	contact
06-I	25	0.25-3	70	1.0-5	5	0.25	0	0	Meguma	contact
03-G	0	0	90	5.0-10	10	<0.25	0	0	xenolith	near
03-G	10	0.5-2	75	1-5.0	15	0.5-2	0	0	xenolith	near
03-H	10	<0.25-1	80	5.0-25	10	0.25-0.5	0	0	xenolith	near
03-H	10	0.25-1	65	1-20.0	25	0.25-3	0	0	xenolith	near
01-A	20	3	55	0.5-1.5	20	0.25-0.5	ZnS-5	<0.25	SMB	far
02-B	5	<0.25	90	5.0-10	5	<0.25	0	0	SMB	far
040429A	40	0.5-3	0	<0.25	60	0.5-1	0	0	SMB	far
040429B	40	0.25-1	0	0	60	0.25-1.5	0	0	SMB	far
040429C	65	0.25-5	0	0	33	0.25-0.5	PbS-2	<0.25	SMB	far
040429D	70	0.25-2	0	0	29	<0.25-0.25	ZnS-1	<0.25	SMB	far
040429E	30	<0.25-0.5	0	0	70	<0.25-1	0	0	SMB	far
040429F	80	0.25-1.5	0	0	20	0.25	0	0	SMB	far
03-A	100	<0.25	0	0	0	0	0	0	SMB	contact
03-I	5	<0.25	70	5.0-15	25	0.5-1.5	0	0	SMB	contact

Table 3.1. Sulfide mineral sample characteristics.
Grain size and abundance of Meguma, xenolith, and SMB sulfide minerals

16
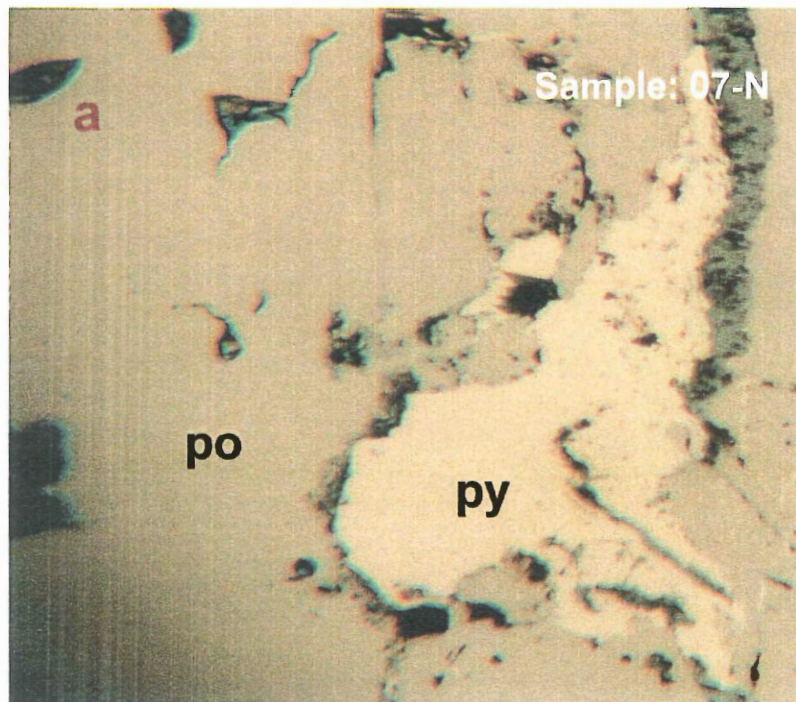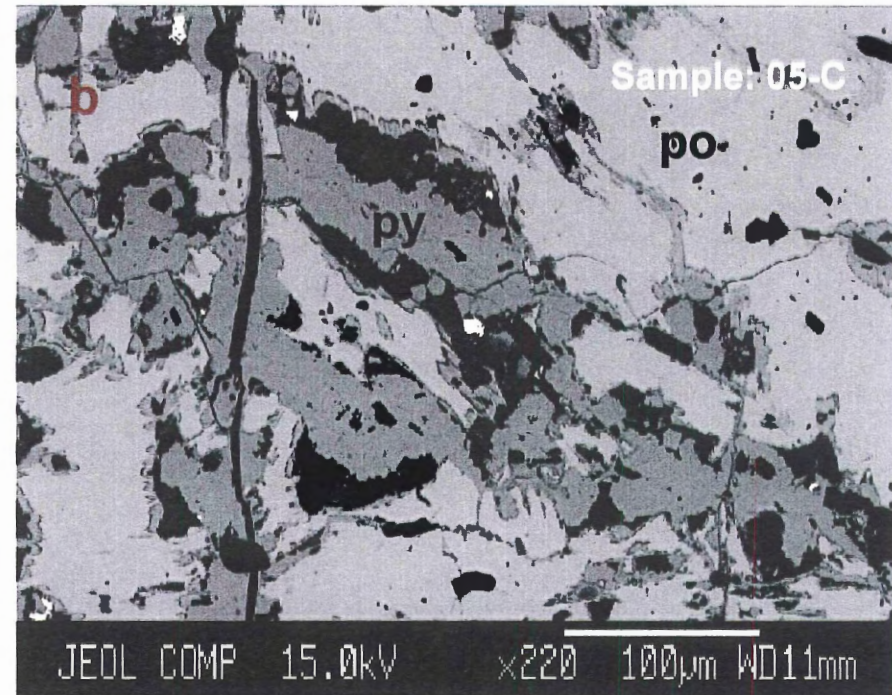
Figure 3.1. Pyrite in the Meguma Supergroup.
a) anhedral, fine-grained pyrite (py), inter-grown with pyrrhotite (po), remote from the igneous contact
b) inter-grown pyrite and pyrrhotite.

17

the igneous contact, pyrite occurs as isolated grains, as well as symplectic intergrowths with pyrrhotite (Fig. 3.1b). At the contact, pyrite grains are anhedral to subhedral and the grain size of pyrite increases, compared with pyrite in the Meguma samples (Fig 3.2).

In this collection of samples, pyrrhotite is the dominant sulfide mineral in the Meguma Supergroup. It occurs as large, anhedral grains, lacking well-developed crystal faces, and commonly contains inclusions of other sulfide minerals, such as chalcopyrite and pyrite. Remote from the igneous contact in the Meguma Supergroup, pyrrhotite exists as fine-grained, poikilitic grains with microscopic inclusions of pyrite (Fig. 3.3b). These sub-rounded grains are commonly disseminated throughout the Meguma samples (Fig. 3.3a). Table 3.1 demonstrates that pyrrhotite is the most abundant sulfide mineral phase in the Meguma.

Chalcopyrite occurs throughout the Meguma Supergroup and SMB as a fine-grained accessory mineral. It occurs as irregularly shaped, anhedral grains contained within larger pyrite and/or pyrrhotite grains. Grain sizes range from <0.25-3.0 mm, however, the majority of the observed grains are <0.25-0.5 mm (Table 3.1). In the Meguma, remote from the igneous contact, chalcopyrite is rare; however, it does occur as very fine-grained inclusions in pyrrhotite. The shape of the chalcopyrite is anhedral in these localities (Fig. 3.4a). Towards the igneous contact, chalcopyrite grain size and abundance increase (Fig. 3.4b).

Three other trace sulfide minerals occur in our study area: arsenopyrite, sphalerite, and galena. These minerals occur as inclusions in larger pyrite and/or pyrrhotite grains, are fine-grained (≤ 0.25 mm, Table 3.1), and vary in shape from euhedral to subhedral. Sphalerite and galena occur rarely in the Meguma Supergroup and as fine- to medium-
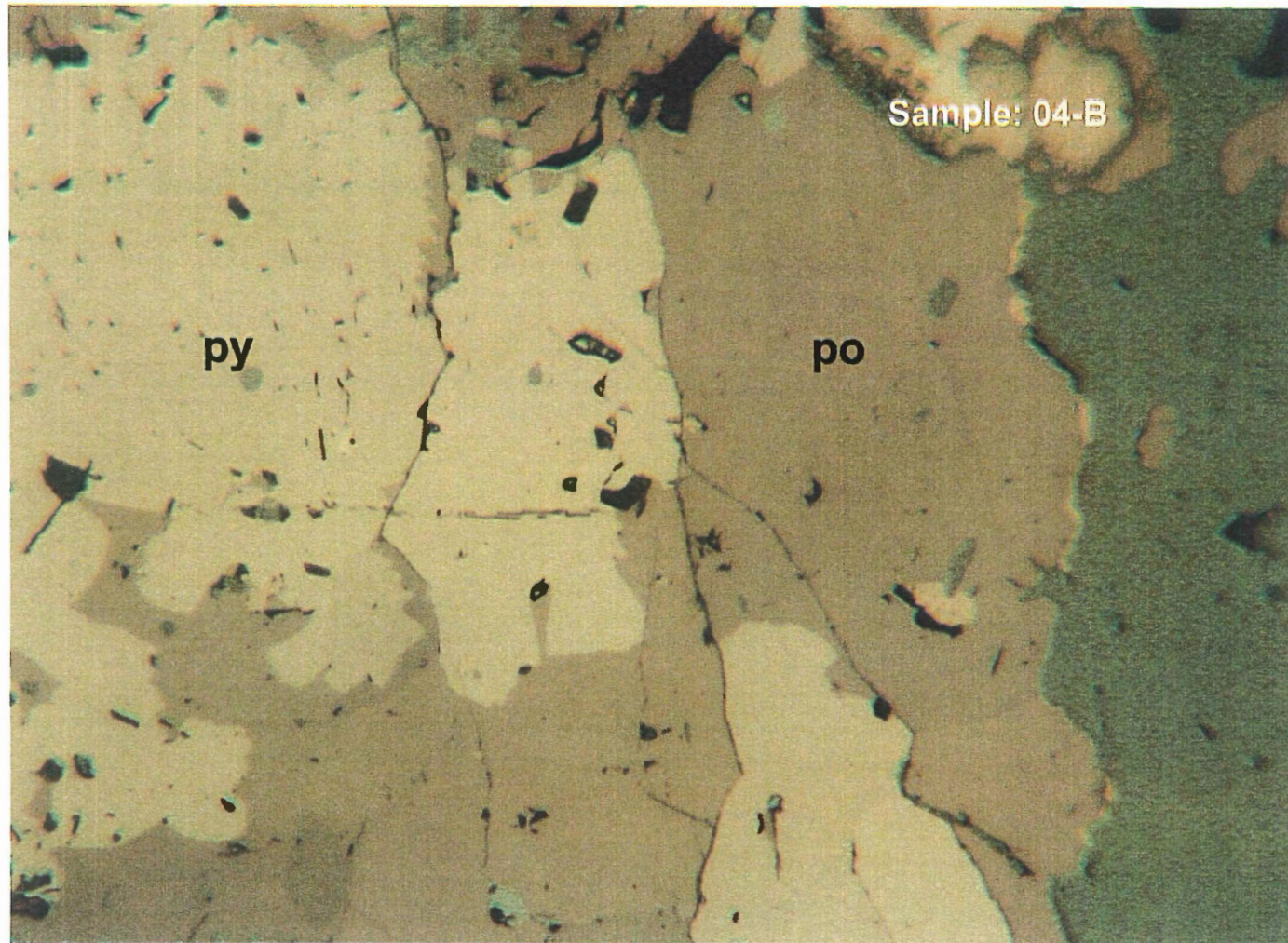
Figure 3.2. Pyrite in country-rock xenolith in granite.
Subhedral pyrite grains with partially developed crystal faces, occurring within large pyrrhotite grains.
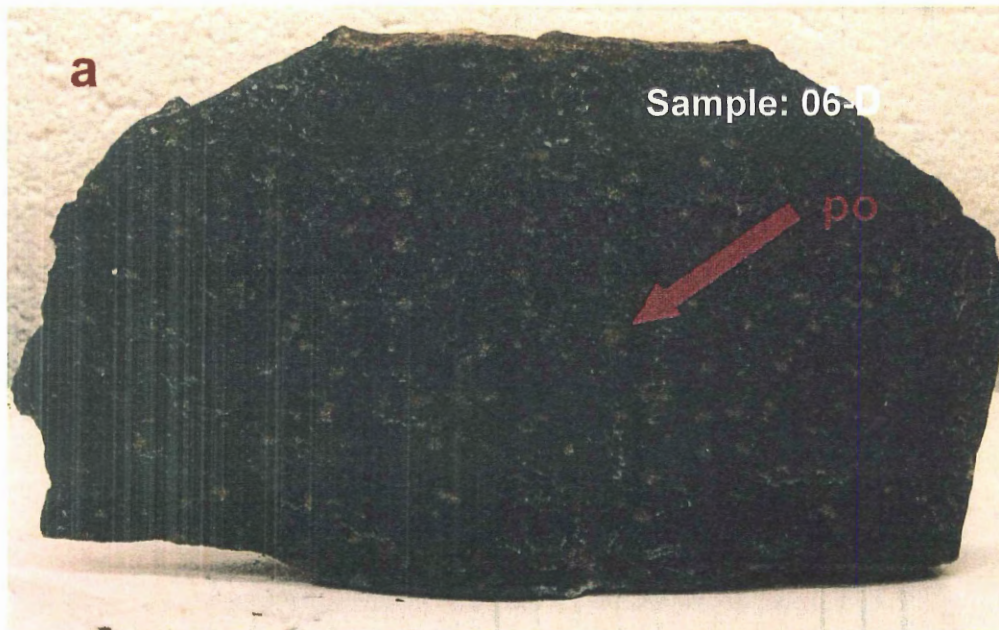
Figure 3.3. Pyrrhotite in the Meguma Supergroup.
a)   disseminated pyrrhotite grains in Meguma hand sample, remote from contact.
b)   poikolitic pyrrhotite grain in the Meguma, remote from igneous contact..
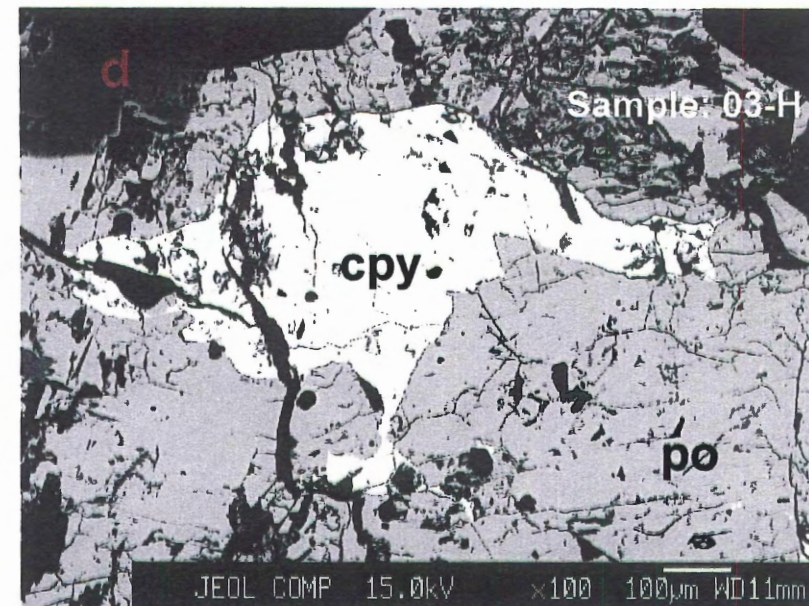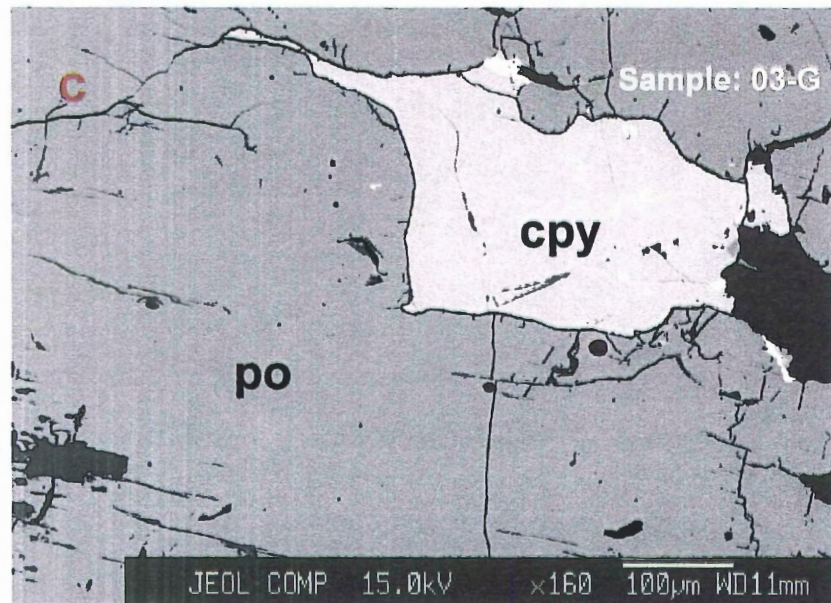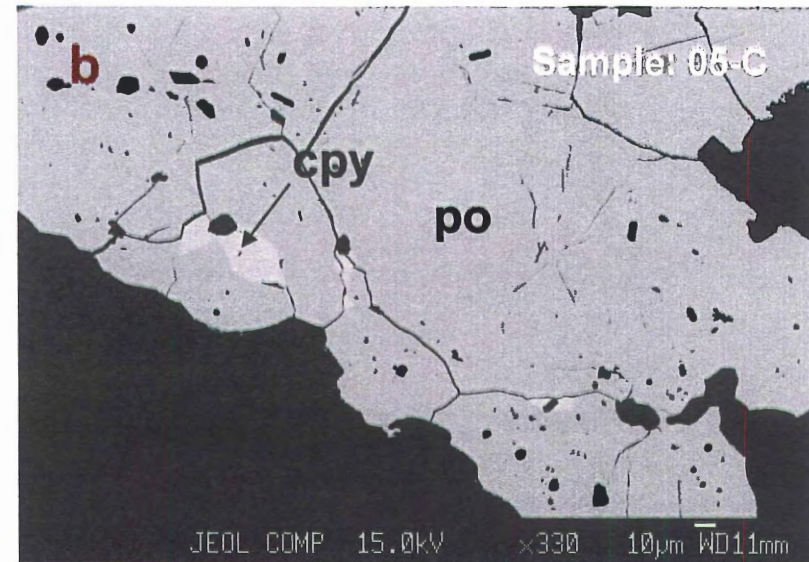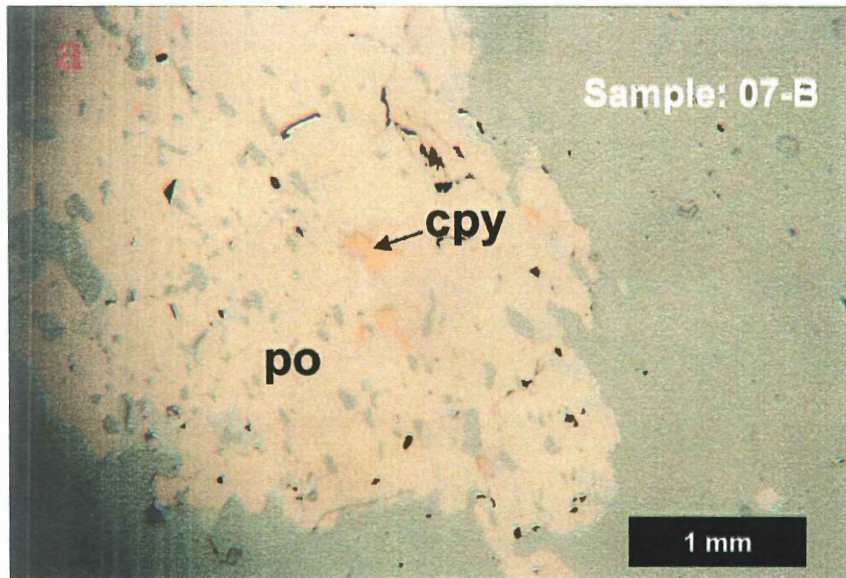
Figure 3.4. Chalcopyrite in the Meguma Supergroup and SMB.
Chalcopyrite (cpy) occurring remote from the contact (a) in the Meguma, close to the
contact (b) in the Meguma, and in the SMB (c,d).

21

sized anhedral inclusions in chalcopyrite, pyrite, and pyrrhotite. Figure 3.5 illustrates sphalerite co-existing with chalcopyrite. Too few grains were encountered to determine any specific relationships as to grain size, crystal habit, and/or abundances.

Arsenopyrite occurs only in the Meguma samples, mostly located close to the igneous contact. They occur as subhedral to euhedral grains, both surrounded by pyrrhotite and along the outside of pyrrhotite grains (Fig. 3.6a).

An unknown sulfide mineral occurs in Meguma samples close to the contact of the SMB. The chemical formula is approximately Fe_2S_3 (Appendix A), which lies between the only two common iron sulfides, pyrite (FeS_2) and pyrrhotite ($Fe_{1-x}S$). Figure 3.6b demonstrates the mottled, fractured texture associated with this mineral.

3.2.2 Textural features of sulfides in xenoliths

In country-rock xenolith samples in the South Mountain Batholith, pyrite grains are anhedral and are located within larger pyrrhotite grains. Pyrite grain size ranges from <0.25-2.0 mm (Table 3.1), thus there is no increase in grain size compared to Meguma samples. In some cases, pyrite displays a distinct wispy texture within pyrrhotite (Fig. 3.7 a,b). This texture is unique to pyrite in xenolithic samples.

The grain size of pyrrhotite increases progressively to a maximum size in a sample located near the igneous contact, surrounding a xenolithic fragment, where it occurs in sulfide bands up to 75 mm long, and 5-10 mm wide. In some samples, the sulfide bands concentrate at the edge of the xenolithic fragments. In the xenolithic

22
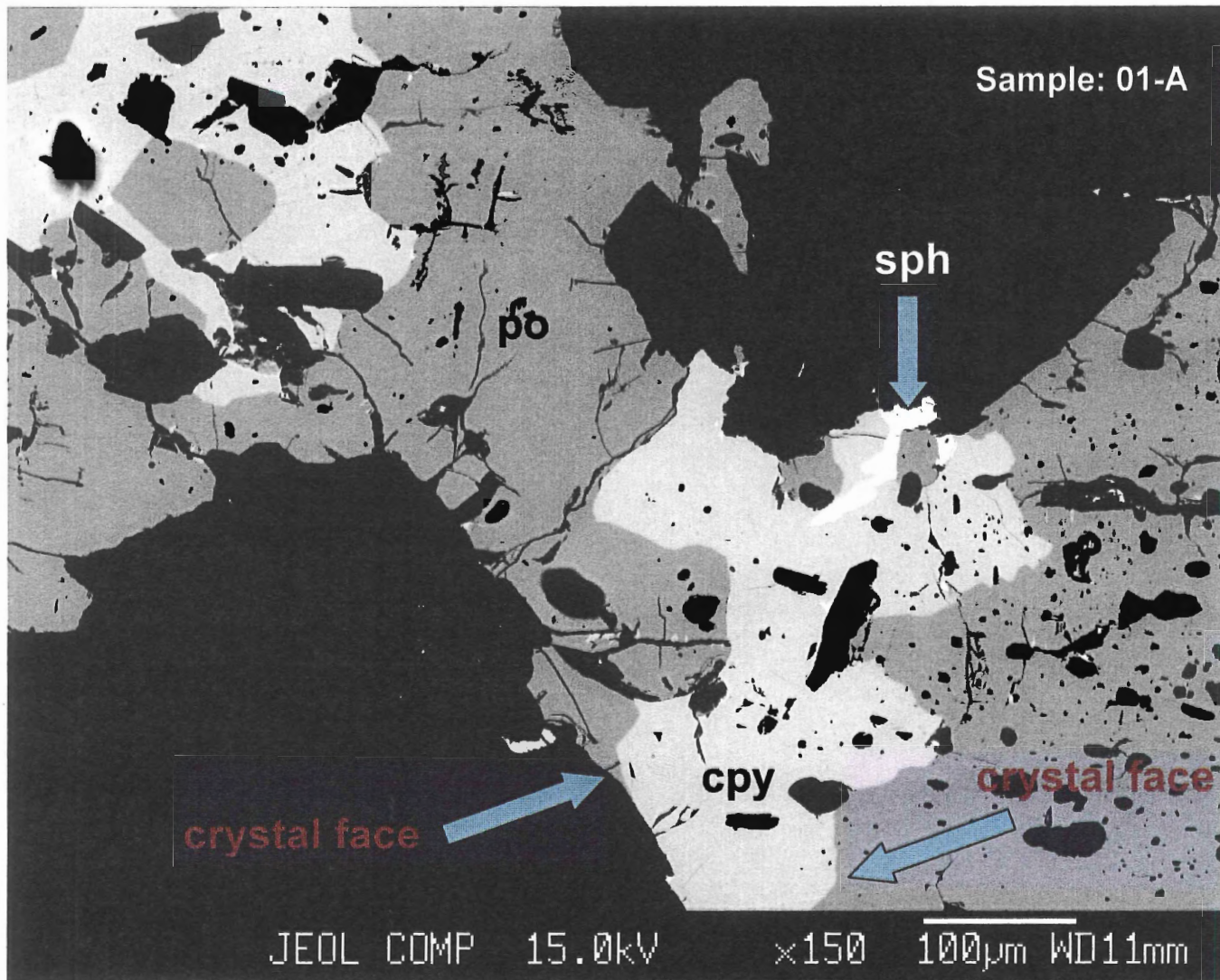
Figure 3.5. Sulfide minerals in the SMB.
Chalcopyrite co-existing with pyrrhotite and sphalerite (sph),
exhibiting partially developed crystal faces.   23
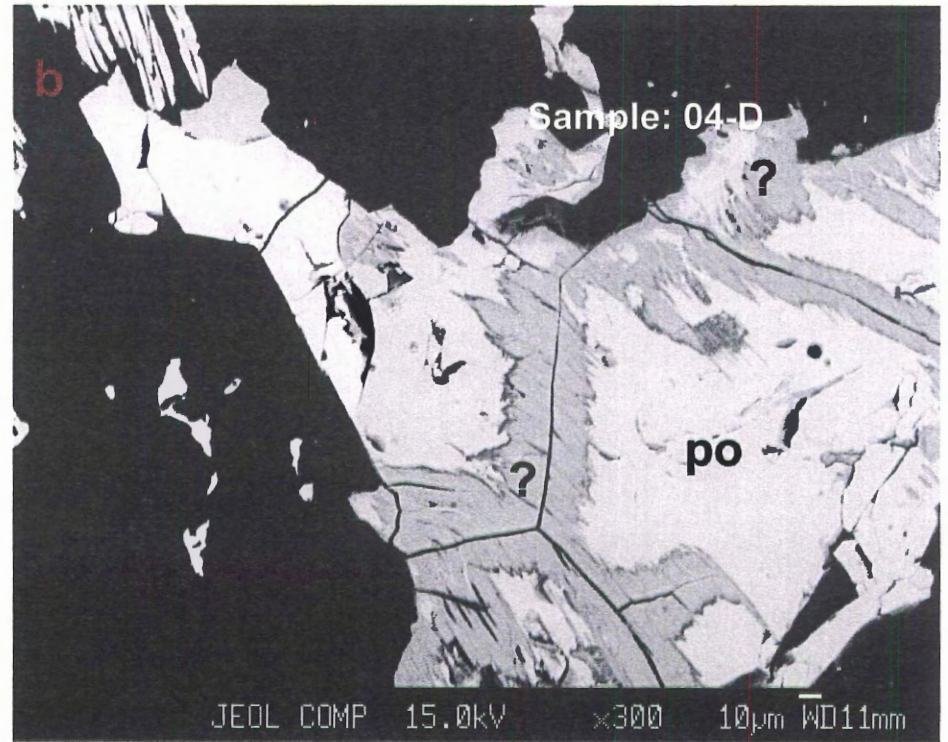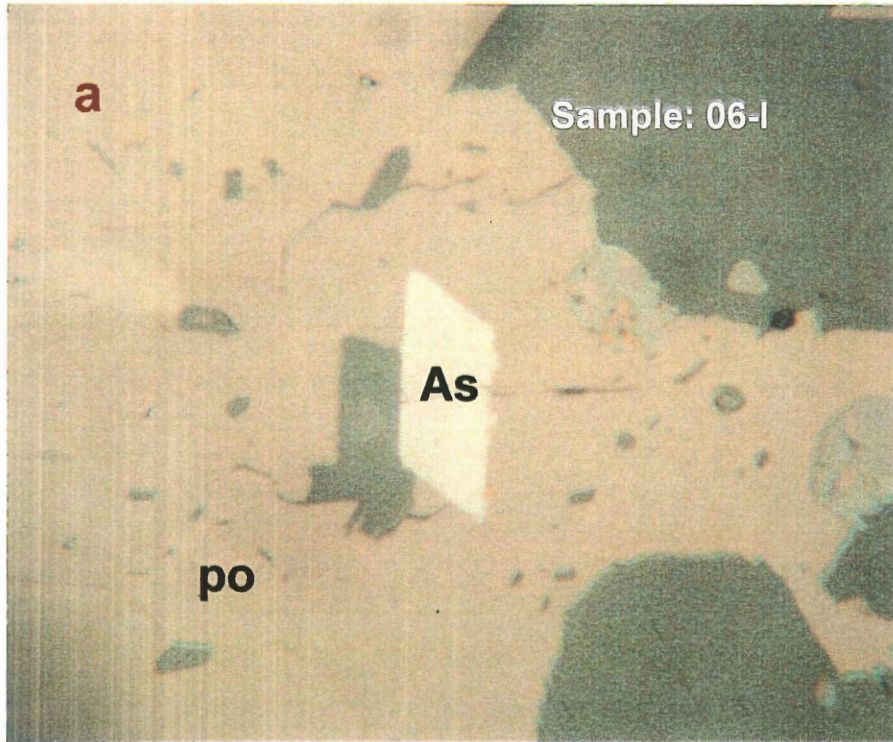
Figure 3.6. Trace sulfide minerals in the Meguma Supergroup.
a)   arsenopyrite (As) occurring with pyrrhotite.
b)   unknown mineral (?) occurring with pyrrhotite.
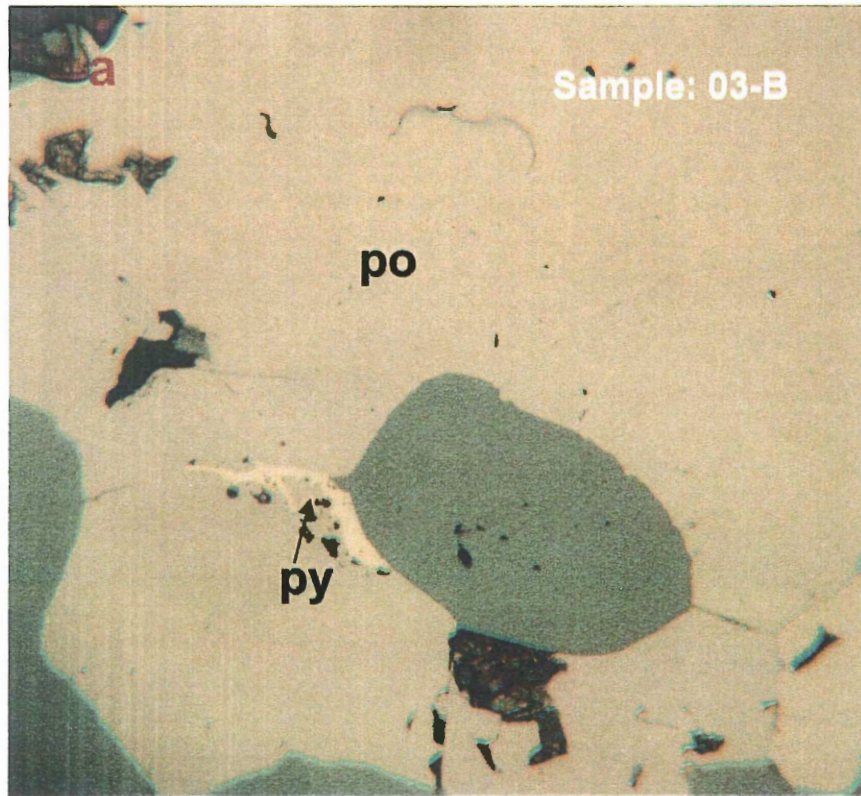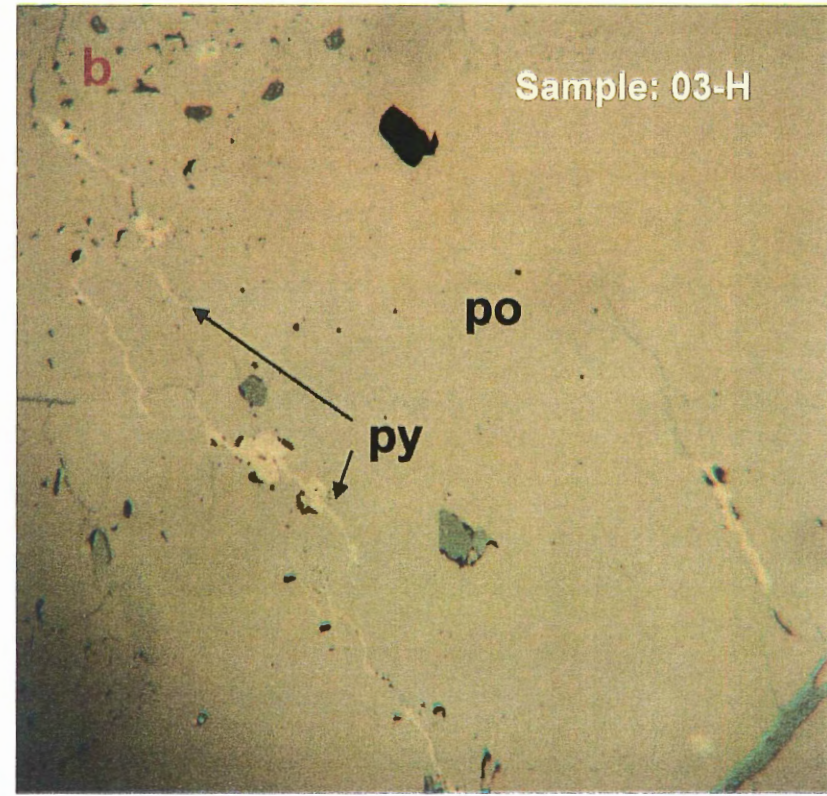
Figure 3.7. Pyrite in country-rock xenolith in granite. Wispy texture of pyrite surrounded by pyrrhotite (a,b).

fragments of country-rock in the South Mountain Batholith, chalcopyrite also exhibits larger grain sizes, as well as a subhedral crystal habit (Fig. 3.4c,d).

The polished hand sample (03-H) is the contact between a metasedimentary xenolith and the South Mountain Batholith granite. Sulfide minerals in this sample concentrate in thick bands along the edge of the xenolith (Fig. 3.8a). Sulfide mineral textures change across the boundary between the xenolith and the granite. In the xenolith, the bands of sulfides are long and continuous with slightly curved grain boundaries. Sulfide minerals in the granite, beneath the xenolith, have a wispy texture and the grains have irregular shapes and grain boundaries. Figure 3.8b shows that the bands of sulfide thin out across the xenolith-granite boundary and the sulfide minerals decrease in abundance in the granite.

3.2.3 Textural features of sulfides in the SMB

In the SMB, pyrite grain sizes are generally larger than in other locations, ranging from <0.25-5.0 mm (Table 3.1); however, no clear trend with respect to abundance exists. Pyrite occurs in the SMB mostly as subhedral (Fig. 3.9a) to euhedral grains (Fig. 3.10a,b). Additionally, pyrite occurs in lamellae structures within pyrrhotite (Fig. 3.9b).

Pyrrhotite occurs in the SMB in varying grain sizes and abundances. Pyrrhotite grains are anhedral in shape and range in size from less than 0.25-5 mm. Table 3.1 shows that the modal abundance of pyrrhotite in the SMB increases in the vicinity of the contact, where it is the dominant sulfide mineral, and decreases further from the contact.

Within the SMB, grain size and abundance of chalcopyrite reaches a maximum. In these locations, well-developed chalcopyrite crystal faces are common as chalcopyrite
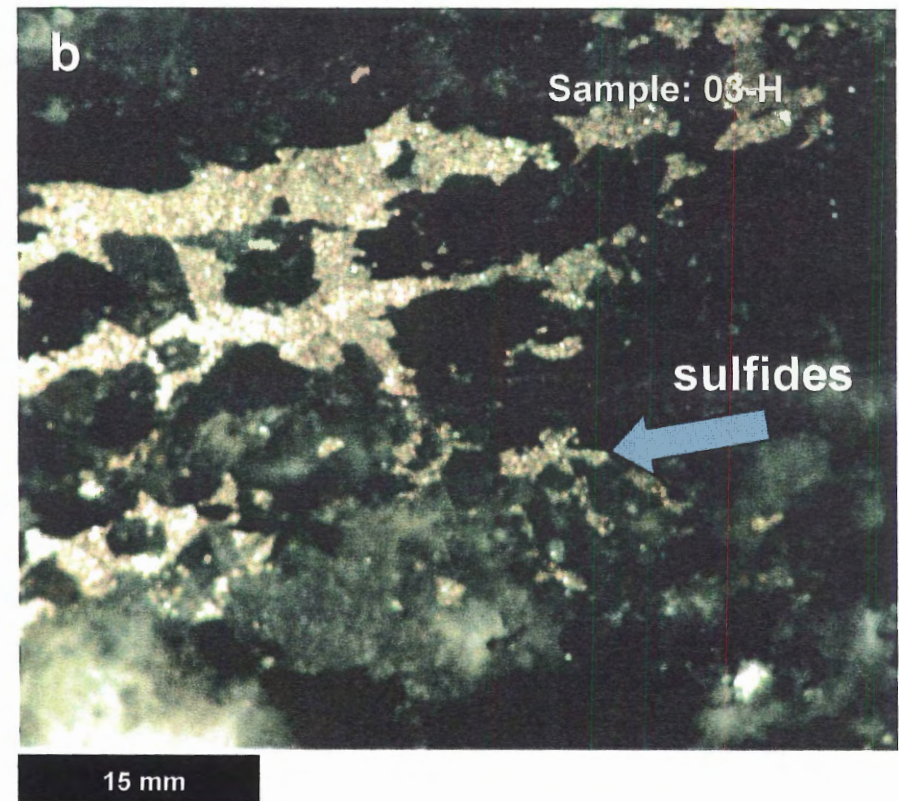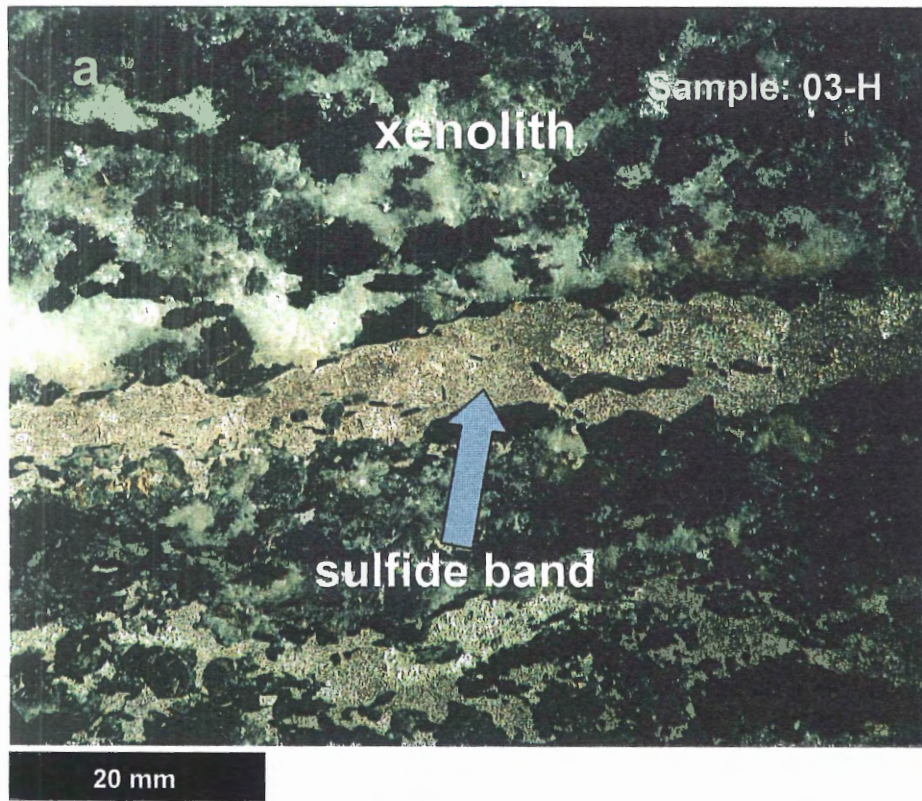
Figure 3.8. Sulfide minerals in country-rock xenolith.
a)   thick band of sulfide minerals concentrated at the edge of the xenolith.
b)   sulfide mineral band breaking apart upon entering the granite.

27
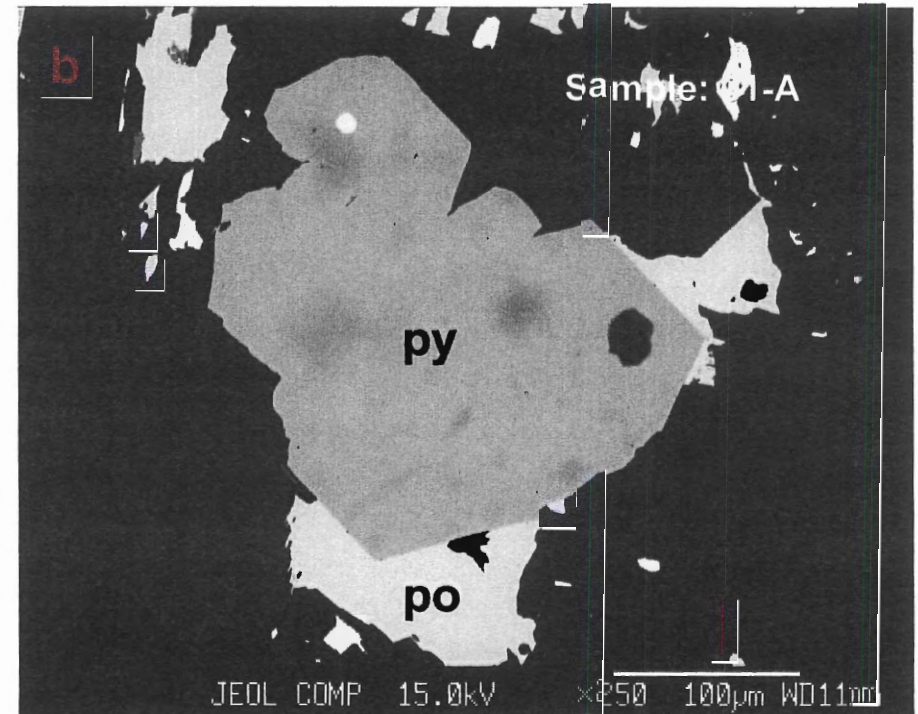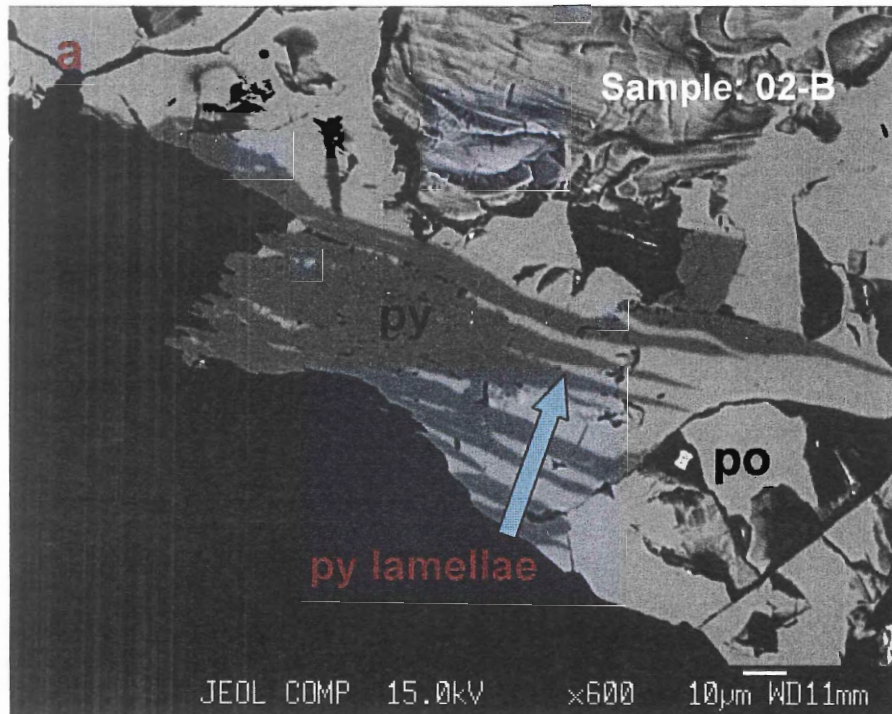
Figure 3.9. BSE images of Pyrite thin sections from the SMB.

a) pyrite lamellae occurring in pyrrhotite.

b) subhedral pyrite grain.
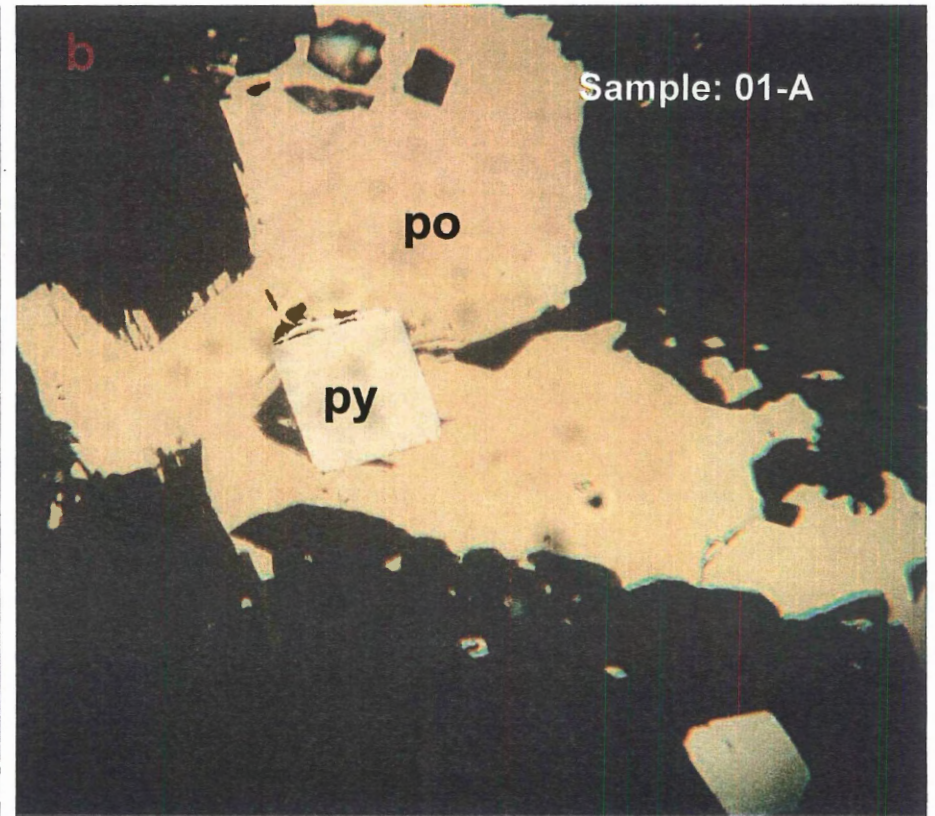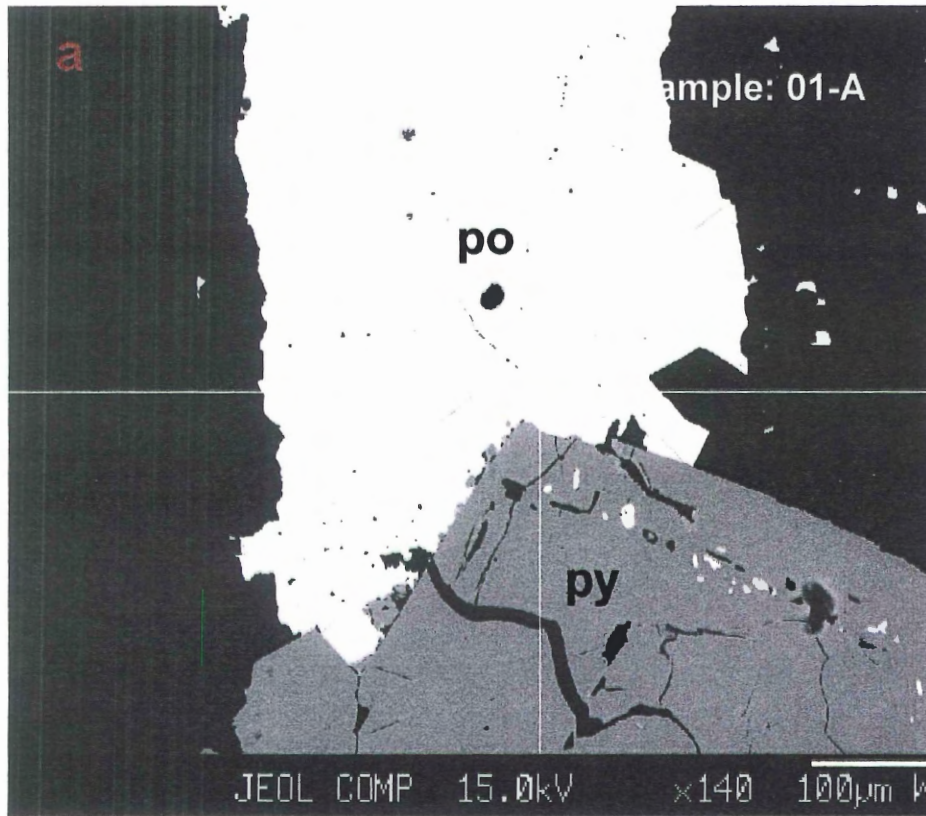
Figure 3.10. Pyrite in the SMB.
Euhedral pyrite grains in a SMB sample (a,b).

29

occurs with pyrite and pyrrhotite (Fig. 3.5). New chalcopyrite crystal habits occur in the SMB, such as the flame texture (Fig. 3.11) that is unique to SMB localities.

Finally, polished sample 03-H demonstrates unique sulfide textures. As mentioned in Section *3.2.2*, sulfide minerals undergo textural changes across the boundary from the xenoliths into the SMB. Further away from the xenolith and into the silicate melt, sulfide minerals are increasingly smaller and rare. Figure 3.12 shows a bleb texture of a fine-grained pyrite in the SMB, which is in close proximity to Meguma xenoliths.

3.3 Mineral Chemical Data

The chemical composition of each sulfide mineral sample was determined through the use of the electron microprobe. Appendix A summarizes the results from the EMP analysis. Figures 3.13 to 3.19 illustrate several chemical relationships.

3.3.1 Pyrite

Appendix A contains the average compositions of pyrite from the Meguma, xenoliths, and the SMB. In the Meguma, the average Fe and S contents are 47.40 ± 1.10 (one standard deviation of Fe content) and 53.20 ± 0.92 (one standard deviation of S content) (wt.%) respectively. The xenolith pyrite samples have average Fe and S contents of 47.46 ± 0.18 and 52.93 ± 0.50 (wt.%), whereas the SMB pyrite samples have average Fe and S contents of 46.36 ± 1.08 and 53.19 ± 0.63 (wt.%) respectively. Figure 3.13 shows a plot of Fe-S in all the pyrite samples. A plot of Ni-Fe in all pyrite samples in Figure 3.14
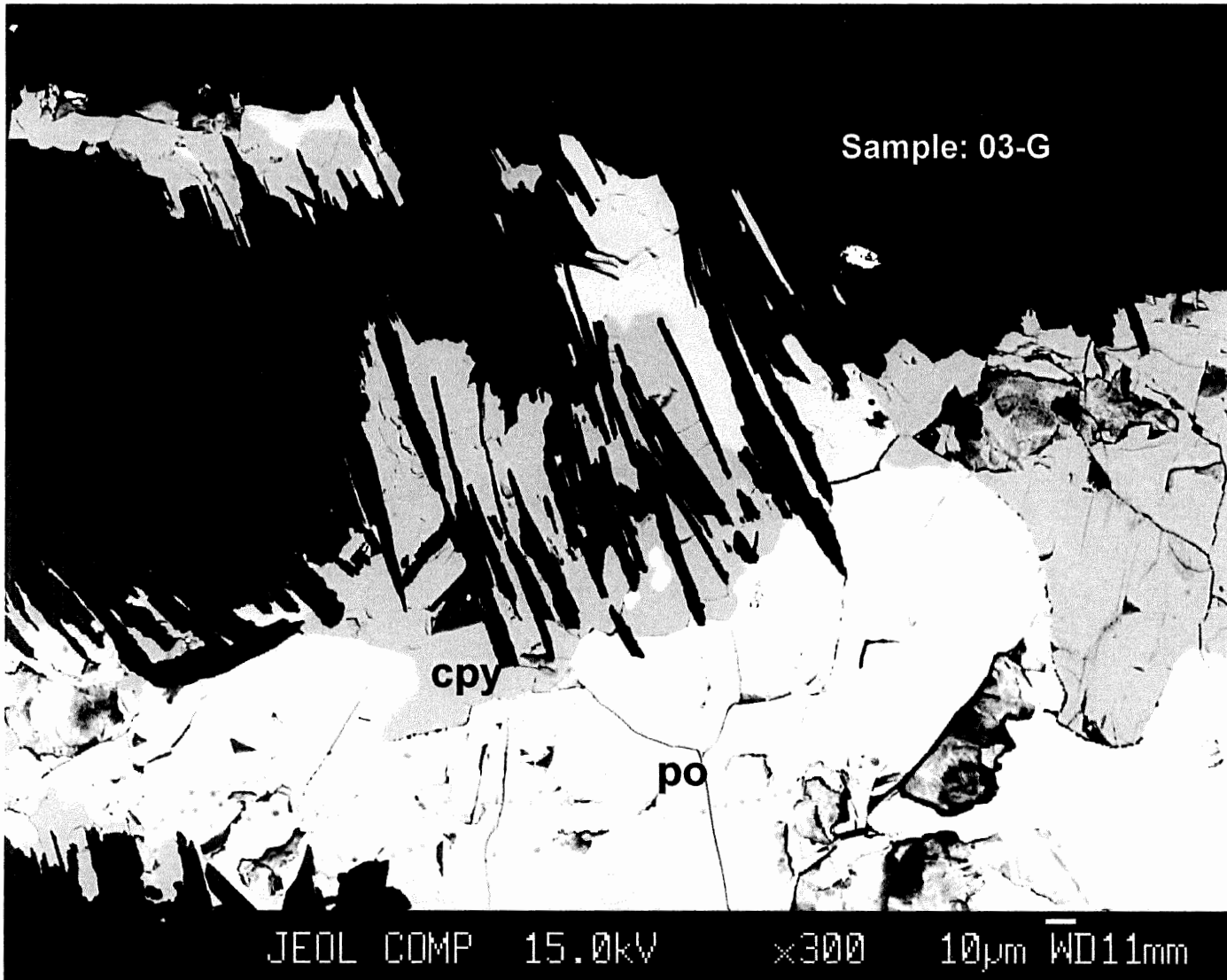
Figure 3.11. Pyrrhotite and Chalcopyrite in the SMB.
Chalcopyrite co-existing with pyrrhotite, demonstrating a structure that is unique
To SMB sulfide samples.

31
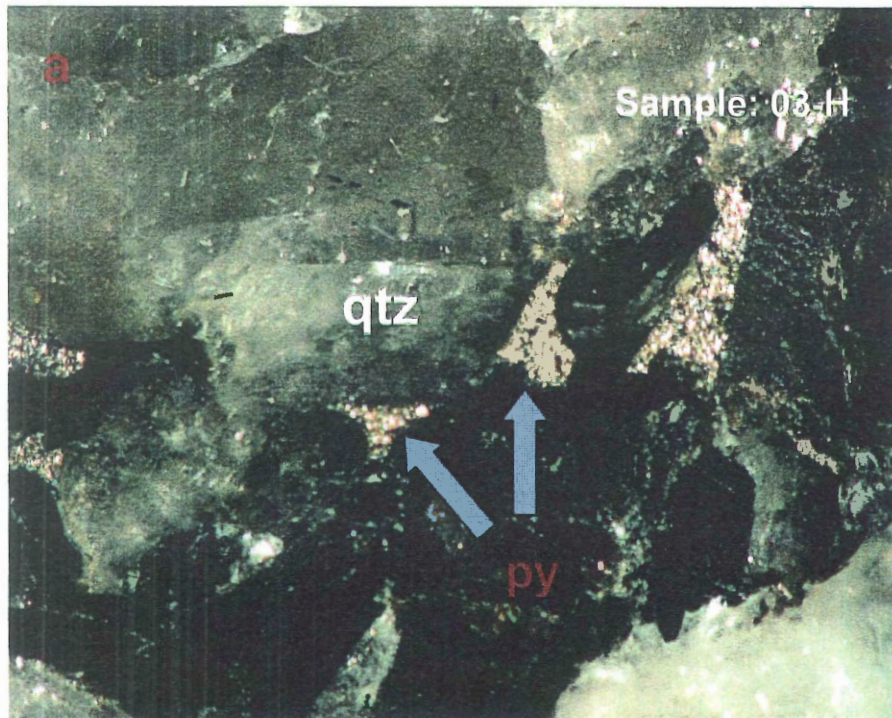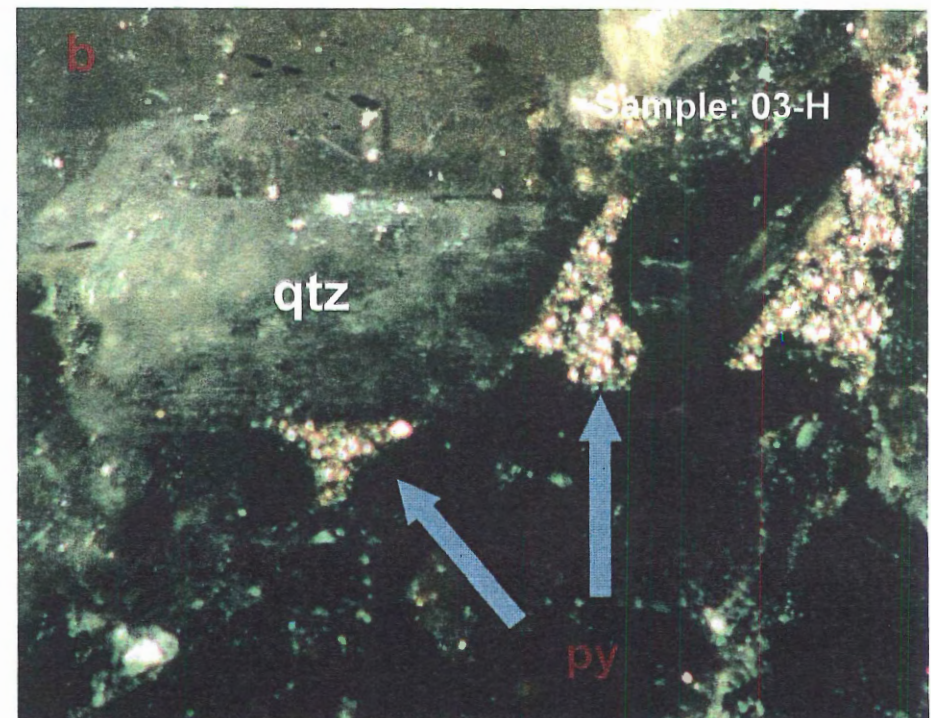
Figure 3.12. Sulfide minerals in granite.
Bleb texture of sulfide minerals crystallizing around quartz (qtz) grain
boundaries (a,b). Cuspate-lobate texture of sulfide mineral follows grain boundaries
of quartz and biotite.
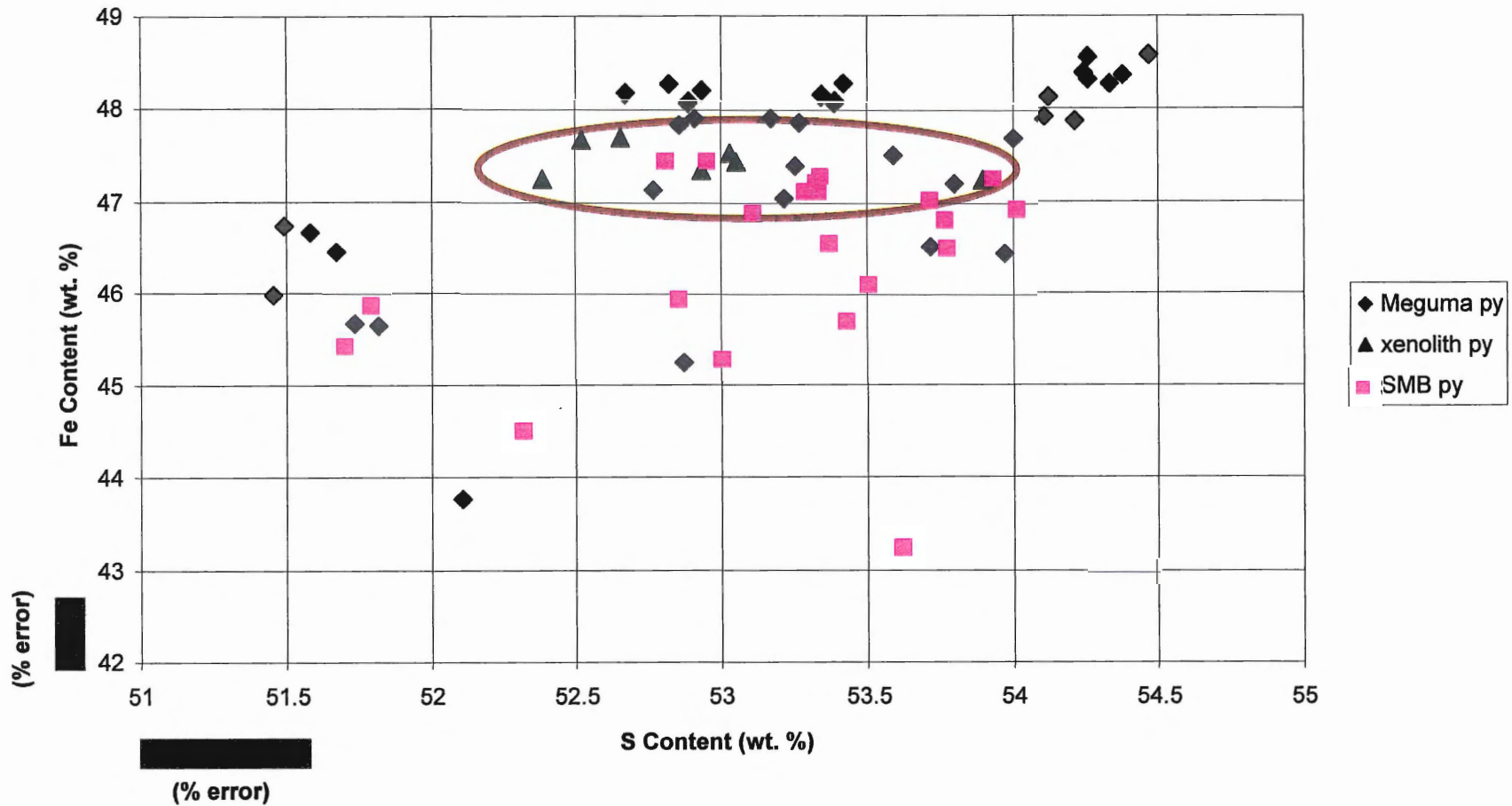
Figure 3.13. Fe-S in pyrite.
The range of Fe content in Meguma pyrite samples is greater than that of SMB samples.
In addition, the xenolith pyrite samples have Fe contents in the middle of the
other two populations.

33
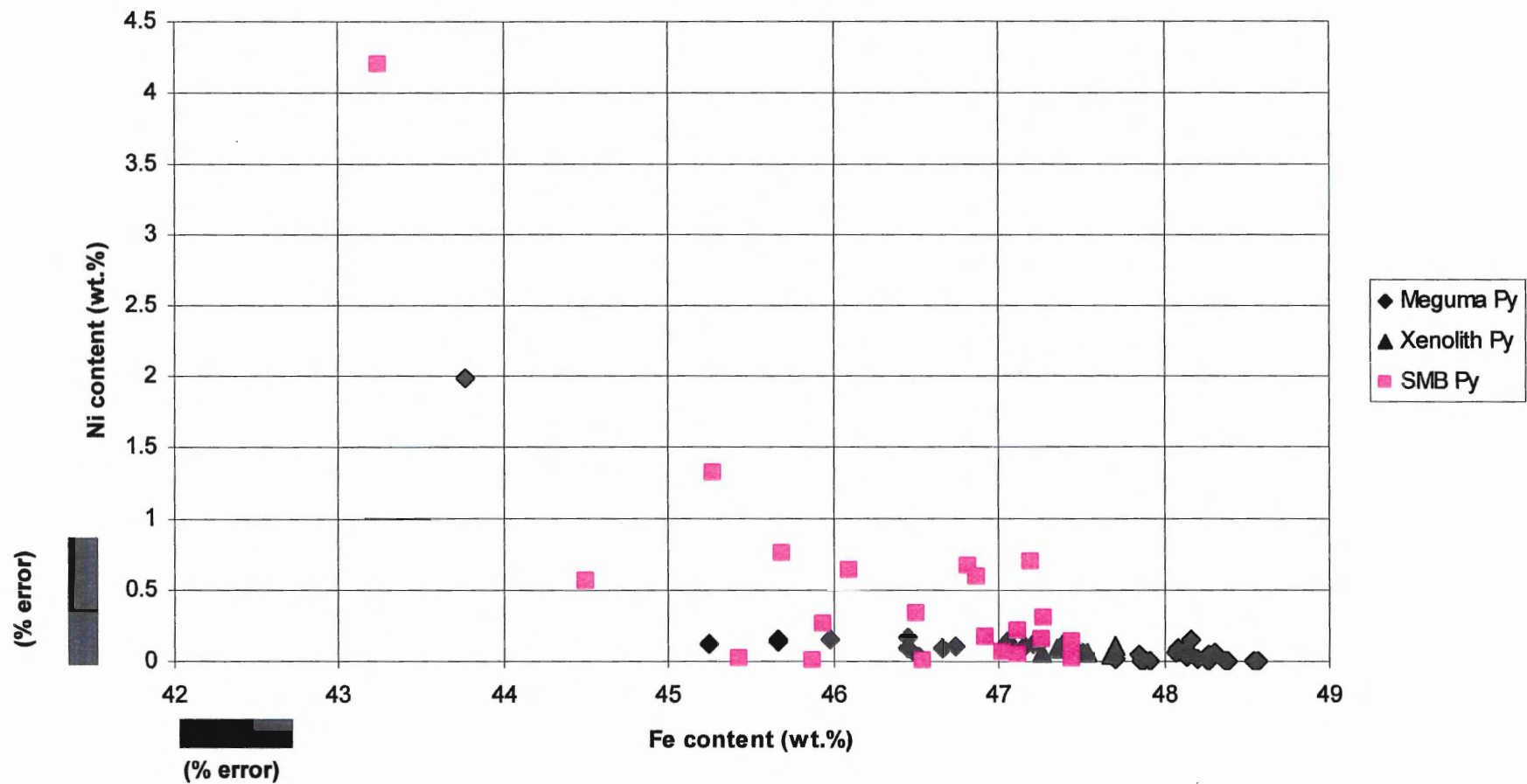
Figure 3.14. Ni-Fe in pyrite.
The Ni contents are higher in the SMB pyrite samples than in the
Meguma samples, with the exception of one anomaly.

34

shows higher Ni contents in some of the SMB pyrite grains compared with pyrite in xenolith and Meguma samples. Finally, Figure 3.15 shows a plot of Cu-S in all the pyrite samples. In this plot, some SMB pyrite samples contain higher concentrations of Cu than xenolith and Meguma samples.

3.3.2 Pyrrhotite

Appendix A displays the average compositions of all pyrrhotite samples. In the Meguma samples, the Fe contents range from 62.64 to 58.02 (wt.%), with an average of 60.52 ± 1.02. The S contents range from 41.26 to 38.23 (wt.%), with an average value of 39.14 ± 0.57. Figure 3.16 illustrates that the range of Fe contents in Meguma pyrrhotite samples is higher than in SMB samples, with the xenolith sample concentrations plotting in the middle of the other two populations. Additionally, a portion of Meguma pyrrhotite exists with a higher Fe content than SMB pyrrhotite samples. A plot of Ni-Fe (Fig. 3.17) shows higher Ni contents in SMB pyrrhotite samples than in Meguma and xenolith samples. Figure 3.18 is a plot of Cu-Fe in all pyrrhotite samples, and shows that some pyrrhotite samples in the SMB and xenolith samples have higher Cu concentrations than Meguma Supergroup samples.

3.3.3 Chalcopyrite

Appendix A shows the average Fe, S, and Cu compositions in wt. % in Meguma chalcopyrite samples: Fe 30.53 ± 0.55, S 35.17 ± 0.31, and Cu 34.45 ± 0.58 (standard deviation of Cu content). The average compositions for xenolith samples are Fe 30.73 ± 0.43, S 35.22 ± 0.40, and Cu 33.85 ± 0.76 and for the SMB chalcopyrites are Fe $30.52 \pm$
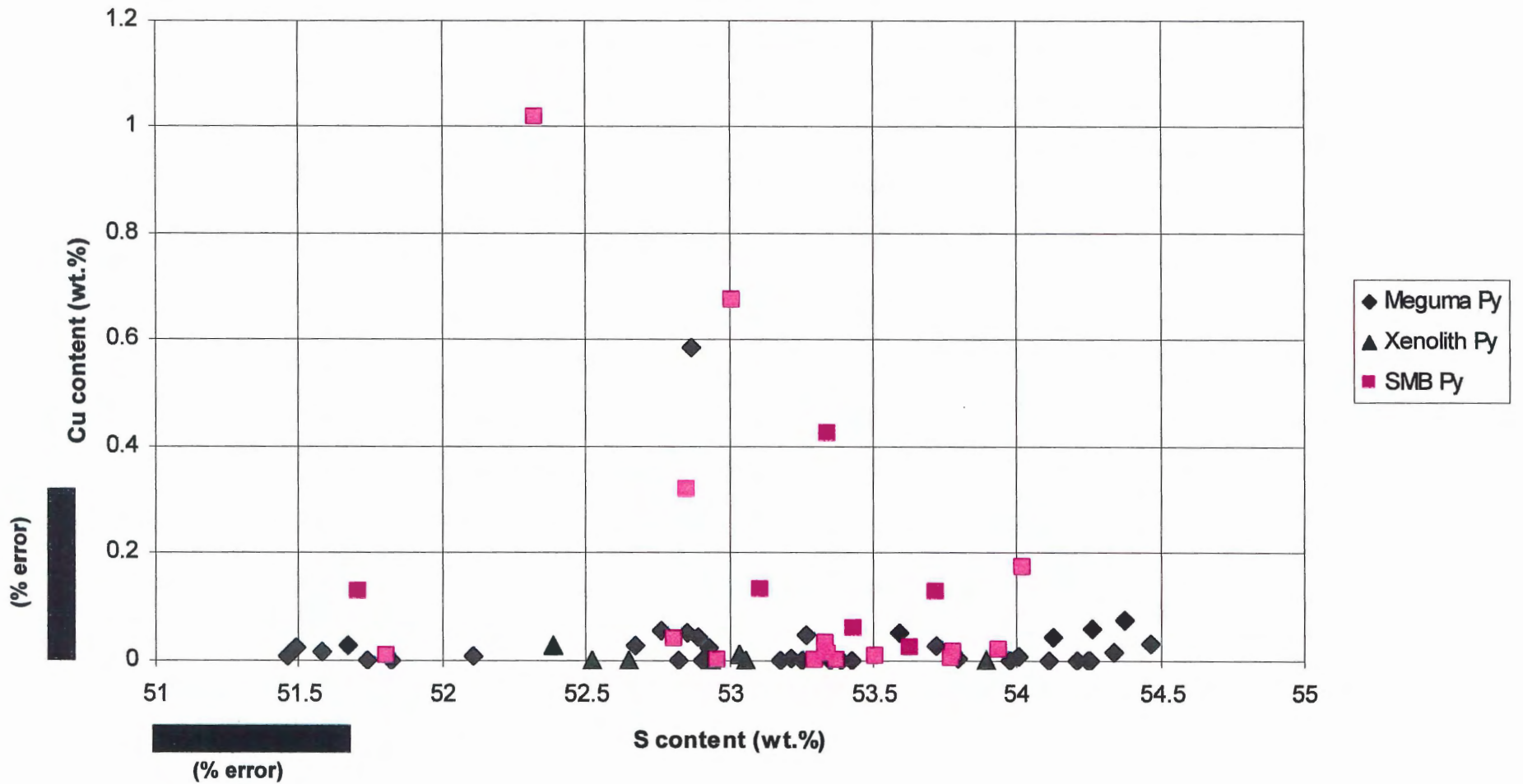
Figure 3.15. Cu-S in pyrite.
Maximum Cu contents in SMB pyrite are greater than that of
Meguma pyrite. Xenolith concentrations closely related to the Meguma samples

36
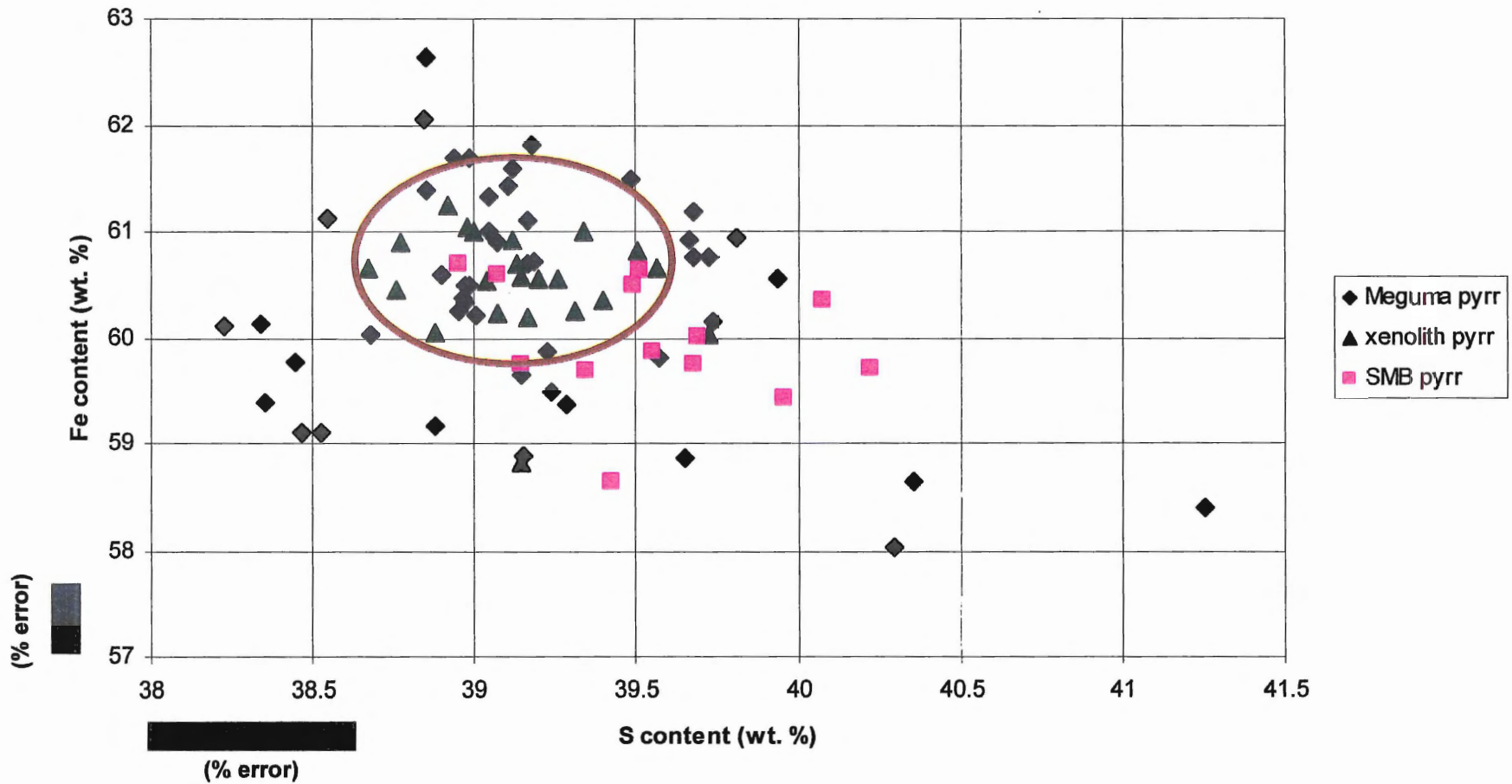
Figure 3.16. Fe-S in pyrrhotite.
Fe contents in Meguma pyrrhotite samples are higher than in SMB samples.
The xenolith sample Fe concentrations plot in the middle of the SMB and Meguma
Populations.
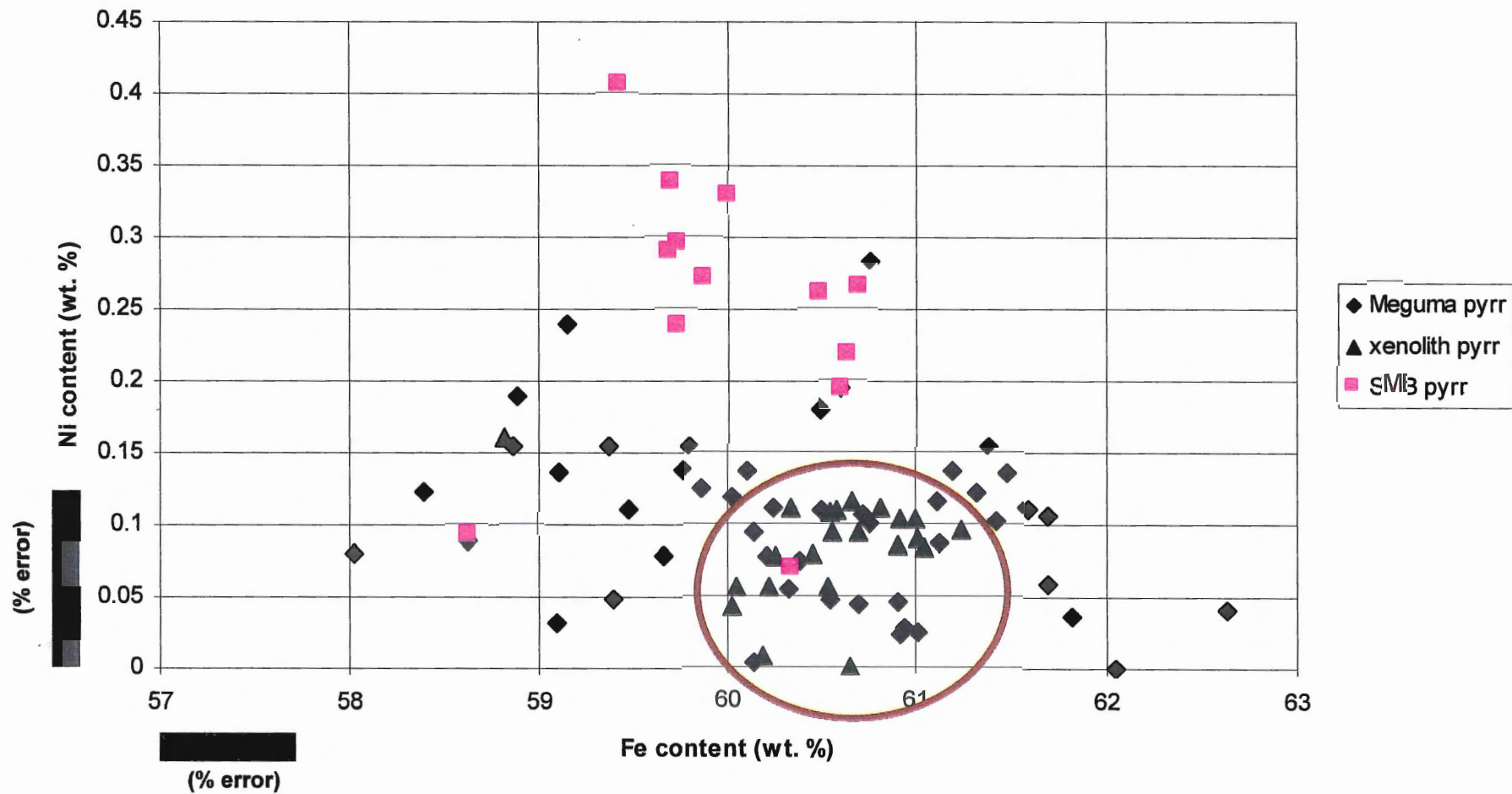
Figure 3.17. Fe-Ni in pyrrhotite.
A general trend exists of lower Ni contents in Meguma pyrrhotite samples than in SMB samples.
Xenolith sample elemental concentrations are similar to Meguma samples
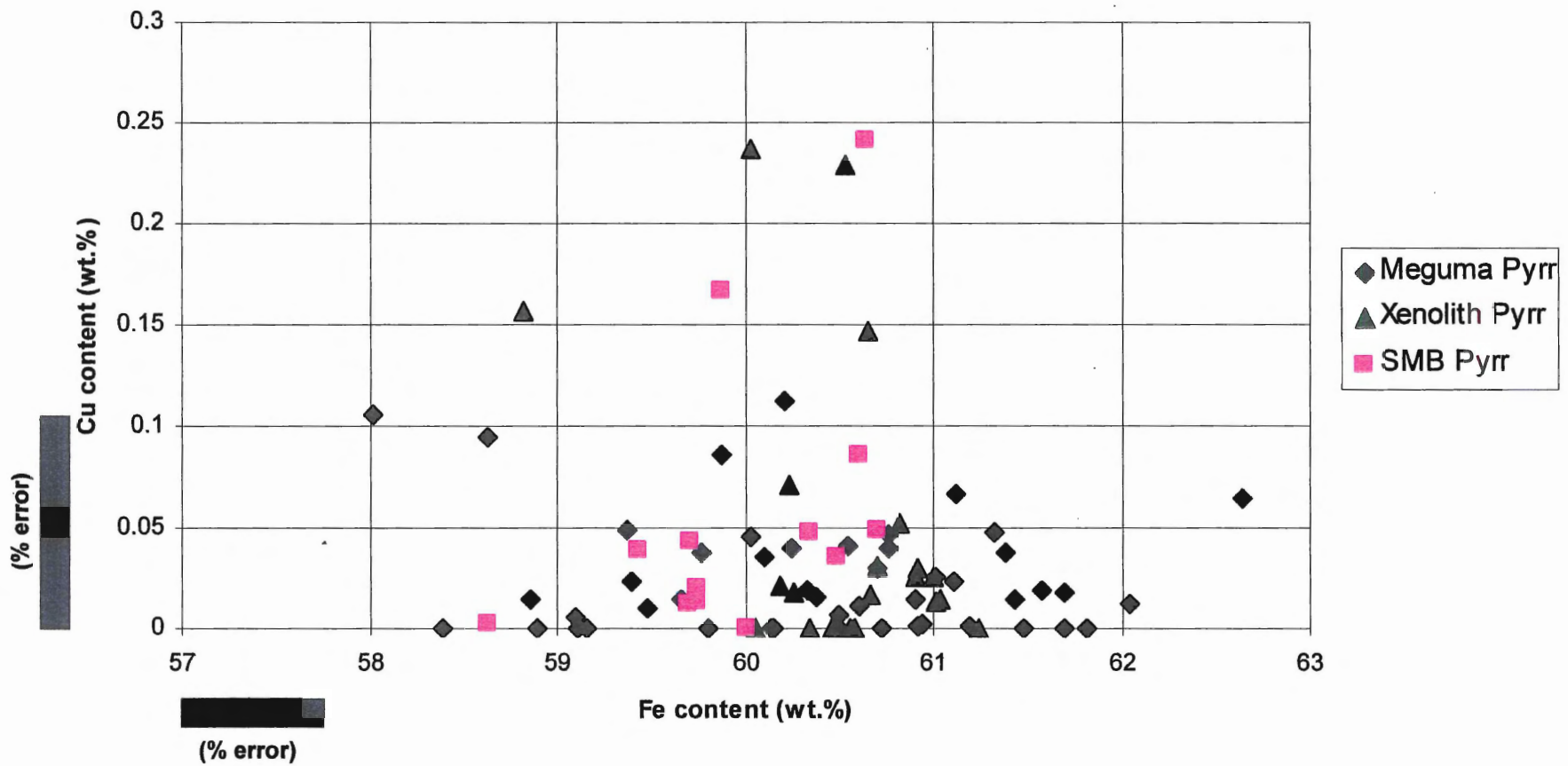
Figure 3.18. Cu-Fe in pyrrhotite.
A portion of SMB and xenolith samples exists with higher Cu content
than Meguma pyrrhotite samples.

39

0.31, S 35.22 ± 0.37, and Cu 34.58 ± 0.56. Figure 3.19 is a plot of Cu-Fe for all chalcopyrite samples, and shows the trend of a higher Cu content in SMB chalcopyrite grains compared with Meguma grains. Additionally, the Cu-S plot shows that the majority of xenolith compositions are closely related to Meguma samples, whereas a small portion with higher Cu contents exists.

3.4 Summary

Several relationships are evident from textural and chemical investigation of the sulfide mineral samples. In the Meguma Supergroup, pyrite and chalcopyrite are fine-grained and anhedral, and pyrrhotite is the most abundant sulfide mineral. Toward the contact of the SMB, and in country-rock xenoliths within the batholith, pyrite, pyrrhotite, and chalcopyrite increase in grain size. Additionally, pyrite and chalcopyrite increase in modal abundance. Finally, within the SMB, pyrite and chalcopyrite grain sizes reach a maximum and crystal faces begin to develop. Nickel contents are higher in SMB pyrite and pyrrhotite samples, and Cu contents increase in pyrrhotite and chalcopyrite samples. Chapter 4 interprets all of the above relationships.

CHAPTER 4: DISCUSSION

4.1 Introduction

Investigation of the textural and compositional features of sulfide minerals yields

several trends regarding their metamorphic and igneous evolution. Textural analysis of

sulfides in hand samples and thin sections provides important information about the

conditions in which the sulfides grew, their crystallization history in relation to

surrounding sulfide and silicate phases, and the source of sulfide minerals in the South

Mountain Batholith. In addition, variations in chemical composition of the sulfide

minerals likely contains information about the conditions of their formation. Finally,

interpretation of the observed trends leads to several models to explain the proportional,

textural, and compositional differences between sulfides in the Meguma Supergroup and

South Mountain Batholith, as well as to determine the origin of sulfides in the SMB.

4.2 Textural variations in sulfide minerals

4.2.1 Textural variations in Meguma sulfides

In the Meguma samples, pyrite, pyrrhotite, and chalcopyrite are most commonly

anhedral and vary in grain size and abundance. Textural features indicate the occurrence

of different processes throughout the history of each mineral. The symplectic texture of

pyrite and pyrrhotite in the Meguma samples (Fig. 3.1b) has two possible explanations.

First, Ramdohr (1980) suggested that such intergrowths indicate a contemporaneous low-

temperature origin of pyrite and pyrrhotite. A second hypothesis is that the texture

represents disequilibrium in a reaction between pyrite and pyrrhotite. It appears that

42

pyrrhotite is replacing pyrite because sulfur can be liberated as a result of heating of Meguma Supergroup rocks near the igneous contact, shown by the reaction:

$$Fe_{1-x} S + FeS_2 \rightarrow 2Fe_{1-x} S + S$$
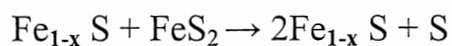
Towards the igneous contact, pyrite grains increase in size and abundance as the metamorphic grade increases. These relationships are to be expected as numerous studies have pointed out a common tendency for pyrite grain size to increase with increasing metamorphic grade (Vokes *et.al,* 1998). The general relationship of pyrite increasing in grain size and abundance is contrary to the above reaction in which $Fe_{1-x}S$ is formed at the expense of FeS_2. The contradiction cannot be explained from the observed textural and compositional characteristics of Meguma Supergroup sulfide minerals.

Throughout the Meguma Supergroup, pyrrhotite is the dominant sulfide mineral. The abundance of pyrrhotite in the contact metamorphic aureole of the SMB and within the batholith is expected as pyrrhotite is stable at high temperature (Ramdohr, 1980). Progressive increases in temperature approaching the contact may be responsible for the subsequent increase in pyrrhotite grain sizes.

Trace amounts of arsenopyrite, galena, and sphalerite occur throughout the Meguma Supergroup and SMB. The occurrence of these accessory sulfide minerals in the samples is so rare that recognition of any relationships relating to morphology, abundance, or phase relationships is impossible.

The presence of one mineral remains difficult to explain. Figure 3.10b demonstrates the atypical, mottled, fractured texture associated with the unknown accessory mineral that occurs close to the igneous contact in the Meguma. The chemical formula is approximately Fe_2S_3, between the only two common iron sulfides, pyrite

43

(FeS_2) and pyrrhotite ($Fe_{1-x}S$). The texture and the location close to the batholith, combined with the unusual formula, may indicate that these grains are the result of submicroscopic intergrowth of pyrrhotite and pyrite.

4.2.2 Textural variations in xenolith sulfides

In the country-rock xenoliths, the morphology of sulfide minerals continued to evolve as new textures exist in these samples. The wispy texture of some pyrite samples is of particular interest (Fig. 3.7). This texture, which occurs only in pyrite located in xenolithic samples, may be the relicts of the symplectic texture of pyrite in pyrrhotite in the Meguma (Fig. 3.1b).

The grain size and habit of pyrrhotite is generally consistent throughout the Meguma Supergroup and SMB. Some exceptions occur, such as in polished sample 03-H, where concentration of pyrrhotite into large sulfide bands occurs at the edge of the xenolithic fragment (Fig. 3.8). The large bands of sulfide minerals, mainly composed of pyrrhotite, may be the result of melting of sulfides in the xenolith and segregation into discrete bands.

4.2.3 Textural variations in SMB sulfides

Pyrite occurs in the South Mountain Batholith mostly as subhedral to euhedral grains. The euhedral pyrite texture in pyrrhotite (Fig. 3.10) suggests unrestricted crystal growth in a sulfide melt (see Section 4.4). The pyrite likely crystallized first as the complete faces had to be uninterrupted by the presence of other minerals. Crystallization may have occurred by: i) crystallization of pyrite followed by pyrrhotite from a sulfide

melt, and/or ii) subsolidus crystallization from intermediate solid solution (*iss*). Additionally, in exsolution reactions of pyrite from pyrrhotite, pyrrhotite must have been present initially (Fig. 3.9a).

Figure 3.9b shows partially developed crystal faces in a subhedral pyrite grain that is common in the granite. The retardation of development of the complete crystal is caused by the physical interaction of a growing pyrite crystal coming into contact with other grains. The result is that numerous sub- to anhedral grains are located within the South Mountain Batholith compared to relatively few perfectly euhedral grains.

Figure 3.9a shows another important texture that occurs in the pyrite in the South Mountain Batholith. The pyrite lamellae produce a flame texture that is characteristic of exsolution. In this case, the pyrite likely exsolved from the surrounding pyrrhotite. The exsolution occurs because in nature, pyrrhotites containing sulfur in excess of Fe_7S_8 will exsolve pyrite during cooling down to 315 ° C (Desborough and Carpenter, 1965). Craig *et. al,* (1998) also pointed out that the primary source of sulfur in pyrite ores is pyrrhotite which releases sulfur during retrograde metamorphism.

Progressive development of crystal faces in chalcopyrite occurs from Meguma, to xenoliths, and into the batholith. The development of the crystal faces in chalcopyrite against pyrrhotite (Fig. 3.5) suggests that the two minerals precipitated simultaneously, likely from a melt as it cooled (see Section 4.4). Studies done by Yund & Kullerud (1966), have shown that co-existing chalcopyrite and pyrrhotite occurs in nature as the Cu-Fe-S system cools below 330 ° C, leading to mineral crystallization from the extensive intermediate solid solution (*iss*) located in the central region of the system (Amcoff, 1981). Figure 3.11 shows further evidence of chalcopyrite evolving from *iss*

45

during cooling, as chalcopyrite lamellae exhibit a flame texture characteristic of exsolution. The exsolution of chalcopyrite from *iss* during cooling is caused by disequilibrium in pyrrhotite that is saturated in Cu (Amcoff, 1981).

Two interpretations may explain the increasing size and abundance of chalcopyrite at the igneous contact, and especially in the South Mountain Batholith:
A. Chalcopyrite grew at the expense of other sulfide minerals during replacement of pyrite and pyrrhotite. This case is unlikely as no textures occur that indicate replacement of pyrite or pyrrhotite by chalcopyrite. In the majority of cases, pyrite and pyrrhotite grain sizes are larger in the SMB than in the Meguma samples. Subhedral crystal faces in chalcopyrite grains indicate that they have either grown first, grew together with pyrite and pyrrhotite, rather than replacing them.
B. The presence of sulfur in the South Mountain Batholith leads to the formation of sulfide minerals, such as chalcopyrite, pyrrhotite, and pyrite; however, excess amounts of Cu are also present in the SMB that must be partitioned into minerals. Copper has a high distribution coefficient (K_D) between sulfide and silicate melts because it is a chalcophile element. During the formation of the primary sulfide minerals in the SMB, excess Cu in the batholith was incorporated into the sulfide melt that crystallizes sulfide minerals (see Section 4.4). Three cases determine where the Cu is partitioned, each dependent on temperature and composition of the SMB in the specific location. In the first case, the high temperature assemblage of Py + Po, Cu content in the melt is low enough to be successfully dissolved in the solid solution that crystallizes pyrrhotite. Yund & Kullerud (1966) showed that the solubility of copper in pyrrhotite exceeds 3 weight per cent at 700 ° C. As a result, pyrrhotite may contain appreciable copper in this situation. In the second

46

case, Cu concentration in the sulfide melt is too large to be taken entirely into the structure of pyrrhotite. Excess Cu is partitioned into *iss* that exsolves chalcopyrite during cooling (Poulson *et. al.,* 1990). In the final scenario, high Cu concentration in the sulfide melt allow for the primary crystallization of $Py + Po + Cpy$.

In the granite, country-rock xenoliths are subject to increased temperatures that affect the sulfide minerals contained within them. Sample 03-H contains thick bands of sulfide minerals. In the granitic portion of the sample, the thickness and abundance of the sulfide bands decreases progressively further from the xenolith (Fig. 3.8). Tomkins and Mavrogens (2003) stated that in a mixed melt, the silicate melt relative can dissolve sulfides if the magma is sulfur-undersaturated. A possible explanation for the decrease in size and modal abundance of sulfides in the SMB compared with the xenolith fragment is that dissolution occurred as the sulfide mineral melts and/or solids chemically interacted with large volumes of silicate magma.

4.3 Chemical variations in sulfide minerals

4.3.1 Chemical variations in pyrite

Pyrite compositions show a number of trends with regards to major and trace element compositions. These trends are used to attempt to correlate crystallization histories and location. Figure 3.13 shows that Meguma pyrite grains have higher Fe contents than those of South Mountain Batholith samples. According to Huston *et.al.* (1995), pyrite can contain high levels of trace elements either as inclusions, or within the crystal lattice. Therefore, the cause of differing Fe contents may be the variable presence

47

of chalcophile trace elements associated with the igneous intrusion, thus leading to lattice substitution for Fe in the SMB pyrite.

Another trend is illustrated in Figure 3.13, where xenolithic pyrite samples plot in the middle of the other two populations. The xenolith pyrite may be interpreted to occur intermediately linking a Meguma sample with no lattice substitution and an SMB sample with abundant lattice substitution. As a result, the xenolithic samples may represent a transitional point where country-rock xenoliths began to react with and assimilate into the magma.

Studies done by Huston *et.al.* (1995) show that one common stoichiometric substitution in pyrite is Fe↔Ni. These substitutions are chemically stable and tend to remain in the lattice during both hydrothermal and metamorphic recrystallization (Huston *et.al.,* 1995). Figure 3.14 shows that SMB pyrite grains have high Ni contents compared to Fe contents. Increased Ni available in the batholith and subsequent substitution during the crystallization of pyrite may lead to decreased Fe contents in SMB pyrites.

Other trace elements occurring in pyrite samples include Zn, Pb, and most notably, Cu; all are *Group 2* elements in the periodic table. Figure 3.15 shows a distinct population of South Mountain Batholith pyrite with high Cu contents. According to Huston *et.al.* (1995), higher concentrations of Cu and other *Group 2* elements are largely the result of submicroscopic inclusions of chalcopyrite (Cu), sphalerite (Zn), and galena (Pb). As previously noted, chalcopyrite increases in abundance within the batholith, thus higher Cu contents in South Mountain Batholith pyrites may be the result of increased number of submicroscopic chalcopyrite inclusions in pyrite grains.

48

The presence of high concentrations of trace elements may also affect the amount of pyrite exsolved from pyrrhotite in the South Mountain Batholith. In general, few cases of exsolution of pyrite from pyrrhotite occur in the South Mountain Batholith (only two in all the samples). According to Yund & Hall (1970), the exsolution rate in natural pyrrhotite is a function of trace element content. If the hypothesis is correct that there are higher concentrations of trace elements in SMB pyrite and pyrrhotite than in the Meguma, pyrite exsolution from pyrrhotite in the batholith may have been sufficiently retarded to make exsolution a rare occurrence.

4.3.2 Chemical variations in pyrrhotite

As in the previous case of pyrite, numerous trends are evident in both the Meguma and SMB pyrrhotite samples with regard to major and trace element compositions. Figure 3.16 shows two distinct populations of pyrrhotite. The Meguma samples have higher Fe contents than the South Mountain Batholith samples, and the xenolithic samples plot in the middle of the other two populations. Two hypotheses may explain this relationship. Each may act on its own or combination with each other:

A: According to Hawley & Nichol (1961), nickel can substitute for iron completely as a lattice substitution in pyrrhotite. Thus, an explanation for decreased Fe content in South Mountain Batholith is Ni substituted for Fe. This explanation not plausible because Figure 3.17 shows that in South Mountain Batholith pyrrhotite samples, the sum of Fe + Ni is not constant. Therefore, one atom of Ni does not replace one atom of Fe, and there must be another explanation.

49

B: An increase in the percentage of Fe in pyrrhotite grains in the presence of pyrite may indicate that exsolution has occurred (Arnold, 1962). Confirmation of the presence of exsolution textures is difficult; however, many more textures occur indicating exsolution of pyrite from pyrrhotite in the Meguma samples than in the South Mountain Batholith samples, especially near the contact of the batholith. As a result, abundant exsolution of pyrite in Meguma pyrrhotite may be the cause of higher Fe contents in the pyrrhotite grains.

Further examination of mineral chemical data for pyrrhotite yields a trend of higher Cu content in South Mountain Batholith and xenolithic pyrrhotite samples compared with Meguma samples (Fig. 3.17). Yund & Kullerud (1959) showed that at elevated temperatures, the solubility of copper in pyrrhotite exceeds 3 weight per cent at 700 ° C, and 2 weight per cent at 600 ° C. The high temperatures encountered by samples in xenolithic fragments located in the South Mountain Batholith may have been sufficient to allow Cu to become soluble in the solid solution that crystallized pyrrhotite (see Section 4.4).

4.3.3 Chemical variations in chalcopyrite

Analysis of the chemical composition of chalcopyrite samples has produced one trend regarding the Cu content of chalcopyrite. Figure 3.19 is a graph of Cu vs Fe in chalcopyrite samples throughout the study area. Two distinct chalcopyrite populations exist in which the South Mountain Batholith samples contain higher Cu (wt. %) than the Meguma samples, and the xenolithic samples fall between them.

A hypothesis has been proposed that may explain the elevated Cu levels in the South Mountain Batholith. First, a change in stoichiometry of chalcopyrite can exist in nature as a result of elevated temperatures, such as those in the South Mountain Batholith (Amcoff, 1981). In addition, Yund and Kullerud (1966) have determined that chalcopyrite in equilibrium with a liquid consisting of sulfur and pyrite becomes increasingly Cu-rich with decreasing temperature. Therefore, a situation in which equilibrium was reached between a sulfide-rich liquid and chalcopyrite in SMB and xenolith samples may have led to the production of elevated Cu levels in chalcopyrite as the magma cooled. The composition of xenolith samples roughly intermediate between batholith and Meguma populations suggests that some xenolith chalcopyrite samples may have been either partially or fully affected by this process.

4.4 Immiscible sulfide liquids

Several authors have noted that sulfide saturation in silicic magmas leads to the formation of immiscible sulfide liquids (Naldrett, 1989, Imai 1994, and Tomkins and Mavrogens, 2003). Naldrett (1989) documented that once a mafic silicate melt is saturated in sulfur, an immiscible sulfide melt evolves. Saturation of silicic magma with sulfide minerals occurs readily because these metals have low solubility in felsic magmas (Tomkins and Mavrogens, 2003). In the SMB, textural and chemical evidence of an immiscible melt exists. Figure 3.10b illustrates a bleb texture of a globule of pyrrhotite in the SMB. A euhedral pyrite grain occurs within the globule. The well-developed pyrite crystal faces within the globule suggest unrestricted crystal growth that may have occurred in the immiscible sulfide melt. Sulfide mineral blebs also occur in the granite,

51

close to xenoliths (Fig 3.12). These sulfide blebs occur interstitially between quartz and biotite grains and their shape depends on the shape of the quartz grain boundaries, suggesting a sulfide liquid crystallized around the contours of an already solid quartz crystal. Imai (1994) noted that the occurrence of sulfide globules suggests that a sulfide melt unmixed from a highly silicic magma. The morphology of the sulfide blebs in the SMB indicates that they are the product of an immiscible sulfide melt. Further evidence of the presence of a sulfide melt occurs in a feldspar grain in the SMB. In this grain, a fracture exists that is filled entirely with sulfide material. The likely explanation for this feature is that the sulfide material was molten as it entered the fracture, occupying all the available space, and then crystallized during cooling.

Chemical evidence of an immiscible sulfide melt is indicated by the trace element chemistry of pyrite and pyrrhotite. Ham *et. al.* (1990) reported that the average concentrations of Ni and Cu in the SMB are 16 ppm and 9 ppm, respectively. Figures 3.14 and 3.18 show concentrations of Ni and Cu, respectively, in SMB pyrrhotite. Chalcophile elements, such as Ni and Cu, appear to be preferentially concentrated in the SMB pyrrhotite samples. A co-existing silicate melt and sulfide melt may provide a source for the excess Ni and Cu in SMB sulfides.

4.5 Sulfide evolution in South Mountain Batholith

The evolution of the South Mountain Batholith has been the subject of study for many authors. Through analysis of the observed sulfide textures and compositions, this paper advances several models for the evolution of sulfide minerals within the South Mountain Batholith (Table 4.1).

The first model proposes a magmatic source of sulfide minerals in the SMB. All of the remaining models propose that the source of sulfide minerals in the SMB is the surrounding, sulfide mineral-rich Meguma Supergroup country-rock. Sulfide minerals undergo a progressive series of textural and compositional changes at locations remote from the contact in the Meguma, towards the contact, and finally into the SMB (Table 4.2). To provide evidence for Models 2-4, a linkage between the country rock and SMB sulfide minerals must be established. Samples taken from xenoliths offer important information as to the origin of sulfide minerals in the SMB.

Model 1

In this model, sulfide minerals in the SMB are not associated with, or affected by, Meguma Supergroup sulfides. Model 1 maintains that sufficient sulfur is present in the magma before it intrudes into the Meguma. As the SMB cools and crystallizes during emplacement, the magma becomes saturated in sulfides and precipitates solid sulfide phases, such as pyrite, pyrrhotite, and chalcopyrite.

Many observations contradict this model. First, sulfide minerals in the SMB are concentrated near the contact with the Meguma Supergroup. The Meguma country-rock is rich in sulfide minerals, suggesting that the Meguma influences the abnormally high concentration of sulfides in the SMB near the contact; therefore, the Meguma is the probable source of sulfide minerals in the SMB (this evidence supports Models 2-4). Second, bands of sulfide minerals extend from Meguma

Sulfide Mineral Source	SMB	Meguma	Meguma	Meguma
	Model 1	**Model 2**	**Model 3**	**Model 4**
Model Description	- sulfur is initially present in magma - as SMB cools, magma becomes saturated in sulfides and precipitates solid sulfide phases	- sulfide minerals occurring in the SMB are entrained xenocrysts - xenolithic fragments break off and fall into the magma	- sulfide minerals dissolve in the magma as the SMB assimilates Meguma country-rock material, ultimately saturating the magma in sulfur - sulfides crystallize directly from silicate melt	- sulfide minerals contained in country-rock xenoliths melt and form immiscible sulfide liquids - immiscible melts migrate into the SMB where they come to rest against solid silicates
Evidence For	- sulfide minerals present in the SMB	- sulfide minerals concentrated near Meguma contact - occurrence of sulfide minerals in the SMB contained within biotite grains form Meguma xenoliths - Poulson *et al.* (1990) $\delta^{34}S$ values are consistent with sulfides of Meguma derivation	- sulfide minerals concentrated near Meguma contact - Poulson *et al.* (1990) $\delta^{34}S$ values are consistent with sulfides of Meguma derivation	- sulfide bands running from xenoliths into granite - bleb texture of globules the result of an immiscible sulfide melt - sulfide minerals concentrated near Meguma contact - Poulson *et al.* (1990) $\delta^{34}S$ values are consistent with sulfides of Meguma derivation
Evidence Against	- sulfide minerals concentrated near Meguma contact - Poulson *et al.* (1990) $\delta^{34}S$ values are consistent with sulfides of Meguma derivation	- bands of sulfide material in xenolith cross into the surrounding granite and begin to break apart as they interact with the magma - chemical evidence of xenolith interaction with SMB	- bands of sulfide material in xenolith cross into the surrounding granite - chemical composition of xenolith sulfides indicates an SMB signature, suggesting interaction of sulfide minerals without complete dissolution	- occurrence of sulfide minerals in the SMB contained within biotite grains from Meguma xenoliths - difficulty in reconciling textural features and melting temperatures of Cu-Fe-S system

Table 4.1 Summary table of models of sulfide mineral evolution in the SMB

	Mineral:					
	Pyrite		**Pyrrhotite**		**Chalcopyrite**	
Location:	Texture	Composition	Texture	Composition	Texture	Composition
Meguma	- avg. grain size <0.25-1.0 mm remote from contact - increasing to 0.5-1.5 mm near contact - anhedral shape - symplectic texture - low modal abundance	- high Fe content - low Cu content - low Ni content	- avg. grain size 1.0-3.0 mm - large, anhedral grains - high modal abundance	- high Fe content - low Ni content - low Cu content	- avg. grain size <0.25 mm - anhedral grain shape - low modal abundance - inclusions within Py and Po	- high Fe content - low Cu content
Xenolith	- avg. grain size 0.25-0.5 mm - low modal abundance - anhedral to subhedral shape - wispy texture in places	- moderate Fe content, in middle of SMB and Meguma populations - low Cu content - low Ni content	- dominant mineral in large sulfide bands - bands are 70 mm in length and 15 mm in width - high modal abundance - anhedral grain shape	- high Fe content - low Ni content - low to high Cu content	- avg.grain size 0.5-1.5 mm -anhedral to subhedral crystal shape - moderate modal abundance	- low to high Fe Content - moderate Cu content
SMB	-avg. grain size 1.0-3.0 mm - subhedral to euhedral grain shape - high modal abundance - lamellae structures in Po suggesting exsolution	- low Fe content - high Cu content - high Ni content	- avg. grain size 3.0-5.0 mm - low modal abundance - anhedral grain shape - bleb textures	- high Fe content - high Ni content - moderate to high Cu content	- avg. grain size 0.5-1.5 mm - anhedral to subhedral crystal habit - flame texture of lamellae suggesting exsolution - moderate modal abundance	- low Fe content - high Cu content

Table 4.2 Summary of textural and compositional variations in Meguma, xenolith, and SMB sulfide minerals.

country rock xenoliths into the SMB granite. These sulfide mineral bands likely formed as the result of partial and complete melting of Meguma sulfides within the xenolith fragment. High temperatures encountered in the SMB magma led to disintegration of the xenolith silicate phases, allowing the dense sulfide melt to drop into the surrounding magma.

Finally, Poulson *et al.* (1990) studied $\delta^{34}S$ variations in Meguma and SMB samples. The study was carried out using samples from the Mt. Uniacke locality, which consists of coarse-grained biotite-muscovite granodiorites of the SMB and metamorphosed graywackes of the Meguma Supergroup. They chose this locality for its high concentration of country-rock xenoliths in the SMB granodiorites (Jamieson, 1974 and Poulson *et al.* 1990). Results of the investigation showed that Mt. Uniacke metasedimentary samples show $\delta^{34}S$ values have a large range, +7.0 to + 22.7%, which is a similar range to regional Meguma samples. A wide range of $\delta^{34}S$ values was also observed in SMB samples from Mt. Uniacke; however, in SMB samples, a systematic variation of $\delta^{34}S$ with distance from the granite-country-rock contacts and central xenolith-rich area occurs (Poulson *et. al*, 1990). Poulson *et. al* (1990) suggested that crustal anatexis of Meguma Group metasediments produced the observed S-type granitoids. Variations in $\delta^{34}S$ within these granitoids are likely produced by assimilation of Meguma country rock; thus, Poulson *et. al* (1990) concluded that $\delta^{34}S$ values are consistent with sulfides of Meguma derivation and that the Meguma Supergroup is an important source of SMB sulfide material.

Model 2

The second model advocates that the sulfide minerals occurring in the SMB are entrained xenocrysts. In this model, country-rock xenoliths present within the magma break up during heating and transport. Sulfide minerals contained within the xenolithic fragments break off and fall into the magma (Fig 4.1). Silicate xenocrysts derived from xenoliths do occur in the granite, and the sulfide minerals within them are chemically and texturally unaltered from Meguma sulfides. Evidence for this model includes the occurrence of sulfide minerals in the SMB contained within biotite grains from Meguma xenoliths. Additionally, $\delta^{34}S$ evidence determined by Poulson *et al.* (1990) suggests that the Meguma Supergroup is the source of SMB sulfide minerals.

Some textural and chemical observations of the sulfide minerals in the Meguma and SMB argue against Model 2. Direct support of physical interaction of sulfide minerals between the SMB and Meguma Supergroup was discussed in Sections *4.2.2* and *4.2.3*, where bands of sulfide material in xenolith sample 03-H cross into the surrounding granite and begin to break apart as they interact with the magma. Examination of chemical data from xenolith sulfide samples shows that the chemical compositions in these samples closely match those of Meguma Supergroup samples (Figs. 3.14, 3.15, 3.16, and 3.17); however, three notable exceptions occur where the xenolith sample populations are clearly unique to the SMB populations (Figs. 3.13, 3.18, and 3.19). The
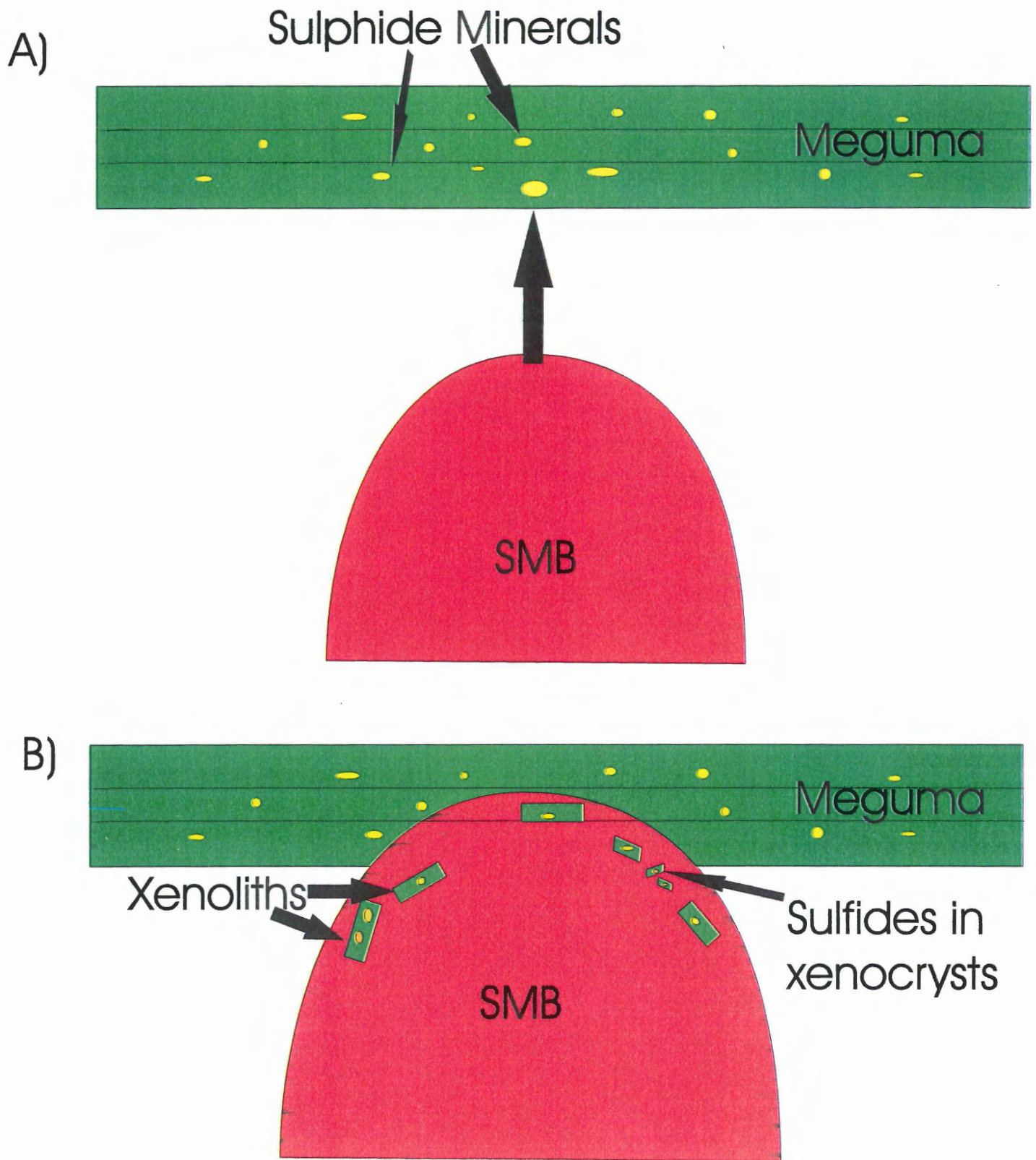
Figure 4.1. Model 2 showing sulfide minerals contained in country-rock xenocrysts.

The SMB intrudes into sulfide mineral-rich Meguma rock. Sulfide minerals within the Meguma are entrained in xenocyrsts, some of which then break up upon entering the magma. The remaining sulfide minerals in the SMB are texturally and chemically unaltered Meguma sulfides.

58

above textural and chemical evidence indicates interaction between sulfide minerals in the SMB and Meguma Supergroup. If the SMB sulfides are xenocrysts, they are chemically modified xenocrysts.

Model 3

Clarke *et al.* (1988) concluded that geochemical diversity evident in the SMB occurred as a result of interaction between the Meguma Supergroup and the SMB during intrusion, as well as assimilation-fractional crystallization (AFC). Through the examination of $\delta^{34}S$ variations, Poulson *et al.* (1990) proposed a model of sulfide evolution in the SMB involving AFC. Model 3 asserts that sulfide minerals dissolve in the magma as the SMB assimilates Meguma country-rock material, ultimately saturating the magma in sulfur (Fig. 4.2). Saturation of the silicate melt potentially in sulfides occurs as the SMB magma cooled, and solid sulfides crystallize directly from the silicate melt.

Problems exist with this model. As discussed in Model 2, xenolith sulfide compositions are clearly in the middle of Meguma and SMB populations, and overlap with the SMB populations (Figs. 3.13, 3.18, and 3.19). The chemical composition of xenolith sulfides indicates an SMB signature, suggesting interaction of sulfide minerals without complete dissolution. Bands of sulfide minerals can be traced uninterruptedly from the xenoliths into the granite; therefore, some of the sulfide minerals originating from country-rock xenoliths must not have entirely dissolved and are clearly present in the granite.
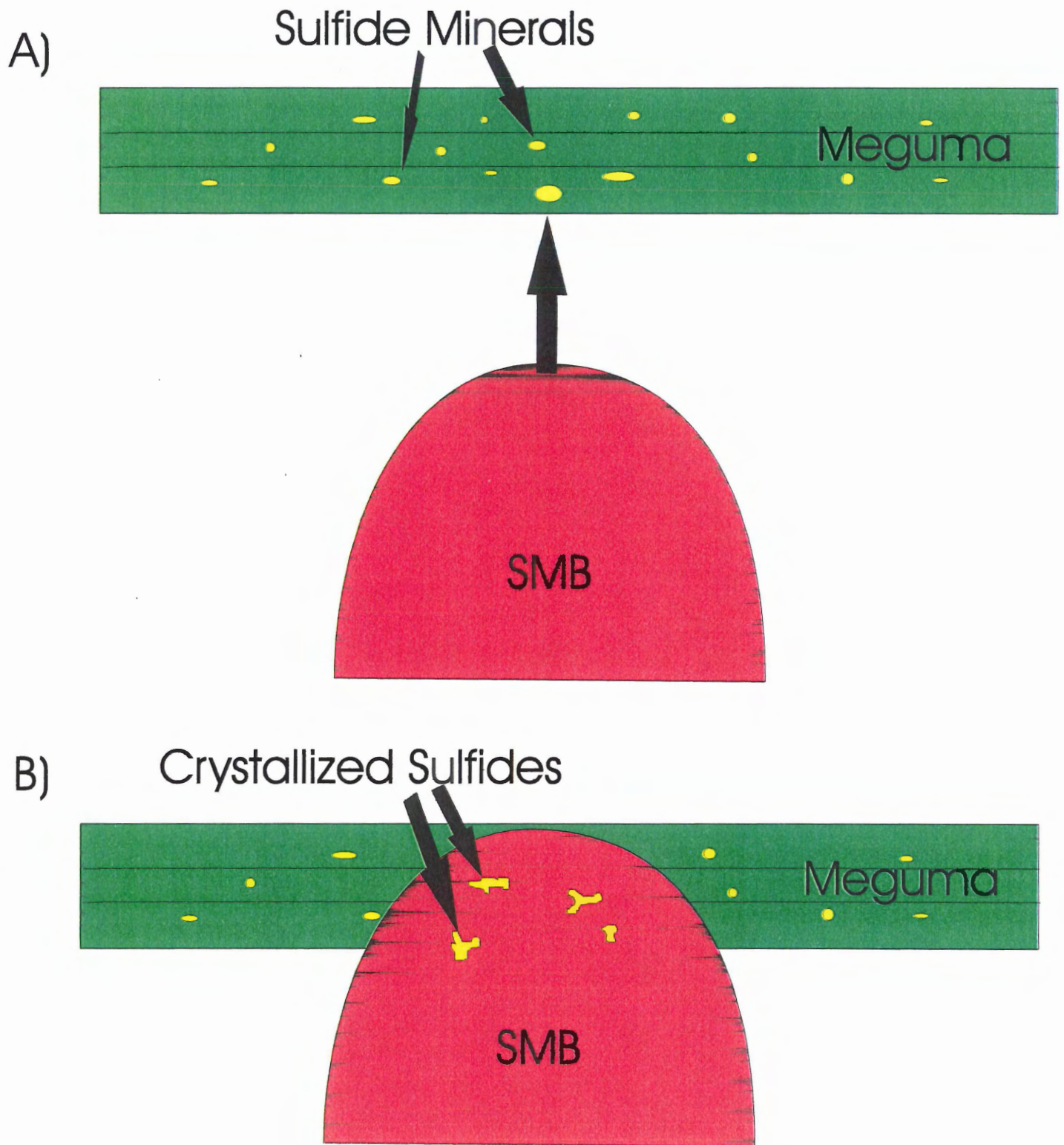
Figure 4.2. Model 3 for evolution of sulfide minerals in SMB showing AFC and crystallization of sulfide minerals from saturated magma. Sulfide minerals in Meguma country-rock undergo complete dissolution in the SMB. As magma cools, it becomes saturated in sulfur and solid sulfide minerals are precipitated.

Model 4

Model 4 states that sulfides in the SMB are the result of partial melting of Meguma country rocks and xenoliths. Sulfide minerals contained in country-rock xenoliths melt and form immiscible sulfide liquids. These immiscible melts migrate into the SMB magma where they break up and partially dissolve (Fig 4.4). The remaining melt crystallizes sulfide minerals during cooling of the SMB.

Textural evidence supports this model. Figure 3.8b illustrates sulfide mineral bands running from country-rock xenoliths into the granite. In the xenolith samples, sulfide minerals are concentrated along the xenolith boundary and decrease in abundance further into the granite where they appear to be dissolving. Furthermore, the occurrence of sulfide globules in the granite in close proximity to xenoliths is evidence for an immiscible sulfide melt (Imai, 1994), which appears to have originated in country-rock xenoliths (Fig. 3.12). These sulfide globules exhibit a bleb texture that appears to be the result of an immiscible sulfide melt that crystallized around solid quartz crystals (Section 4.4). The fracture in a SMB feldspar grain that is filled with sulfide material is further evidence for the presence of an immiscible sulfide liquid (Section 4.4).

This model contains some discrepancies that leave uncertainty in describing the process of sulfide mineral formation in the SMB. The textural evidence for immiscible sulfide droplets in the SMB granodiorite and the (low pressure) sulfide phase equilibrium constraints have been difficult to reconcile. Figure 4.3 shows that the lowest temperature liquid in the system Cu-Fe-S may be ~900°C, considerably higher than estimates of 650–700 °C for the SMB granodiorite magma (Jamieson 1974).
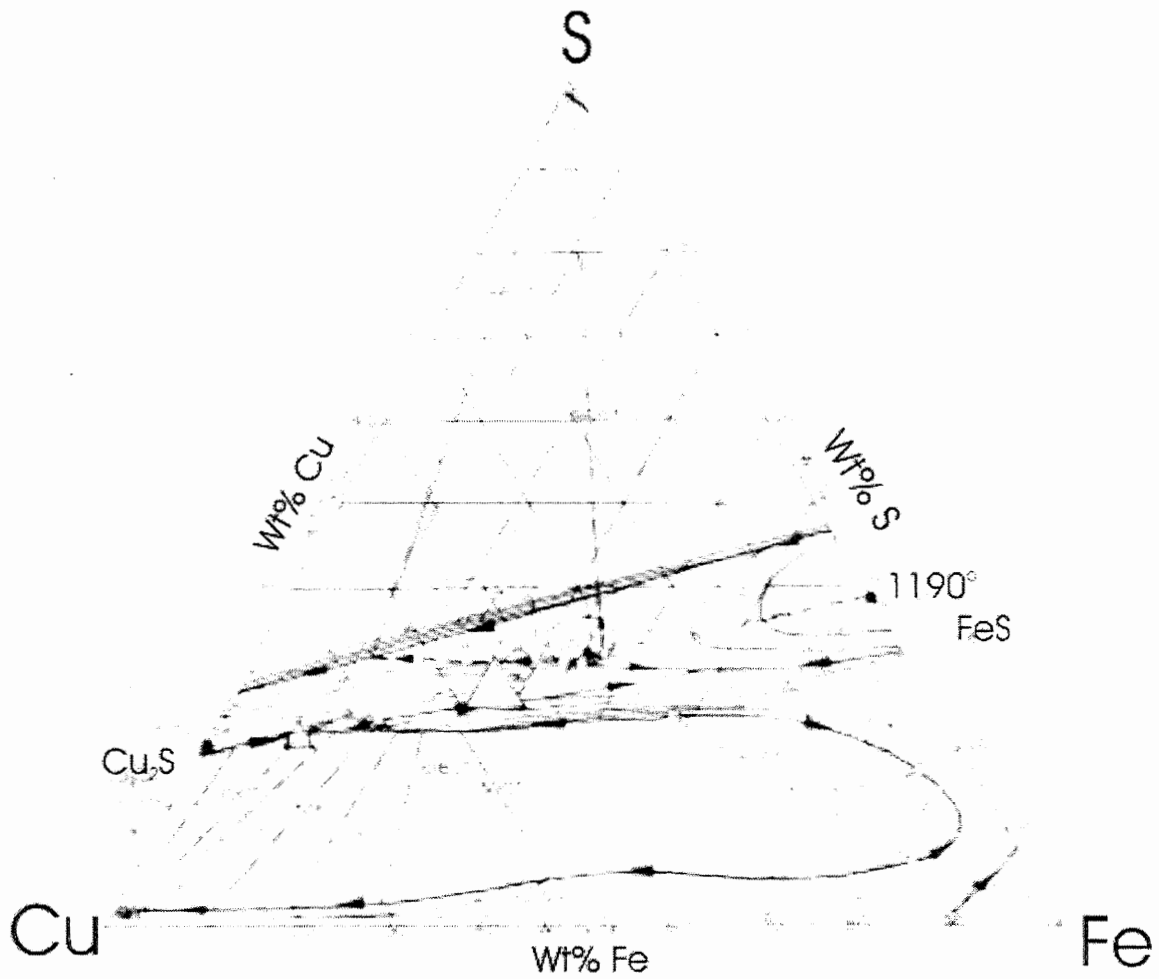
Figure 4.3 Phase diagram of Cu-Fe-S system

In addition, Cabri (1973) showed that chalcopyrite is stable only below 557°C, and that at higher temperatures it breaks down to intermediate solid solution (*iss*). The effect of trace elements within the SMB on temperature and phase relationships of the Cu-Fe-S system is unknown and may modify stability thresholds.
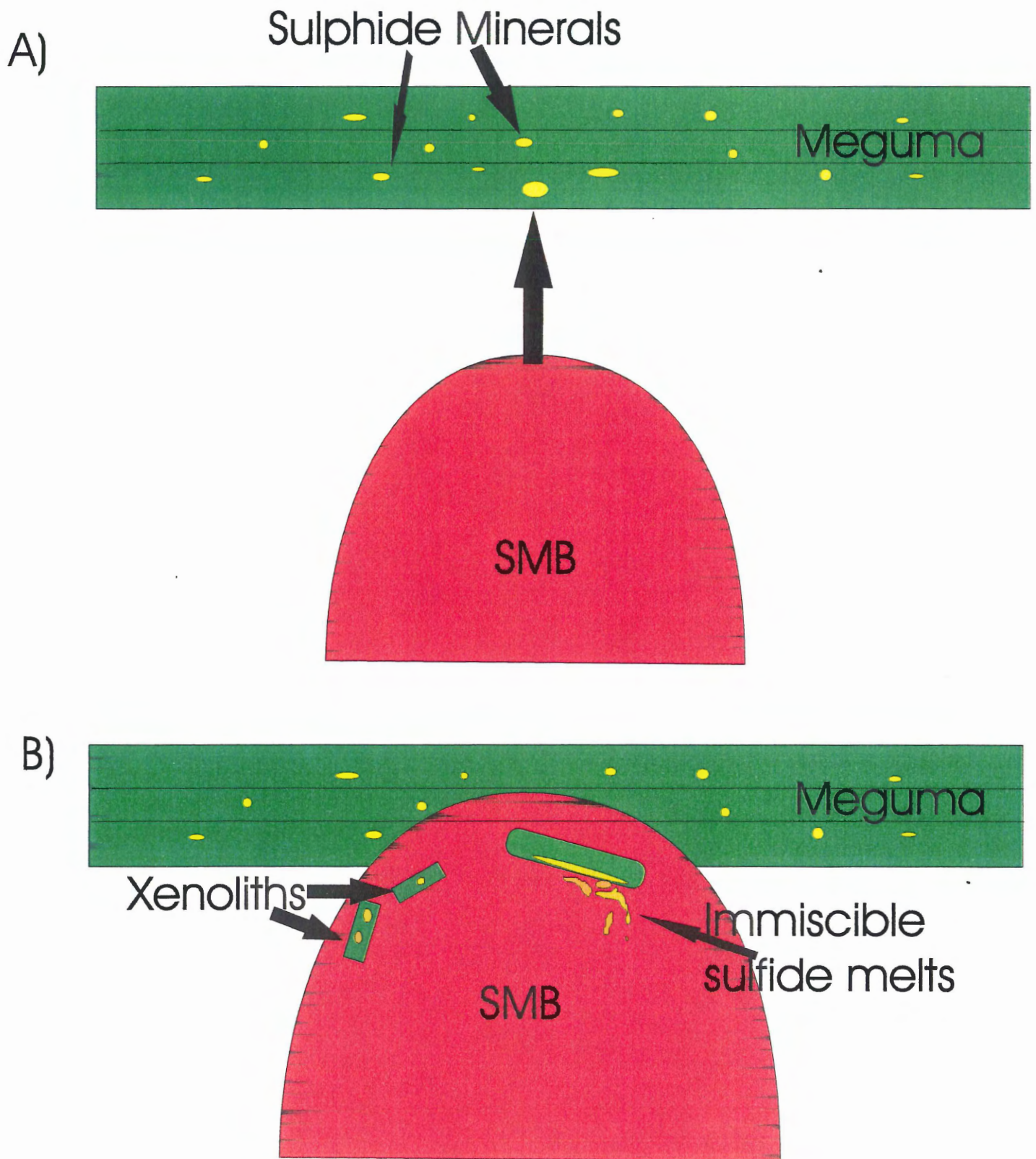
Figure 4.4. Model 4 illustrating that sulfide minerals are melted in xenoliths forming immiscible sulfide melts.

The SMB intrudes into sulfide mineral-rich Meguma rocks. The sulfide minerals in the Meguma rocks undergo partial and complete melting. The resulting immiscible sulfide melts migrate into the SMB, and either dissolve in the magma or crystallize solid sulfide minerals.

63

4.6 Summary

Each of the models proposed in this chapter attempts to explain the observed textural and chemical relationships in sulfide minerals in the Meguma Supergroup, xenoliths, and SMB. Models 2-4 provide the best explanations for the origin of SMB sulfides and the processes they underwent. Each model has its strengths and weaknesses that cannot be ignored; however, Models 2 and 3 contain particular limitations. Given the evidence discussed, Model 4 offers the most complete description for the process of formation of sulfide minerals in the SMB.

CHAPTER 5: CONCLUSIONS

5.1 Conclusions

1. Sulfide minerals in the Meguma Supergroup, country-rock xenoliths, and SMB undergo a series of progressive textural and chemical changes. These changes are the result of high temperature conditions associated with the emplacement of a large-scale igneous intrusion into sulfide-rich country-rock.

2. Textural and chemical evidence from sulfide minerals in Meguma xenoliths indicate that they are intermediate between the Meguma and SMB samples.

3. Textural, chemical, and isotopic relationships indicate that the Meguma Supergroup is the source for sulfide minerals in the SMB.

4. Sulfide minerals contained in country rock xenoliths melted to form immiscible sulfide liquids. These immiscible sulfide melts underwent partial to complete dissolution in the SMB. The remaining melt crystallized sulfide globules in the granite.

5. Enrichment of sulfide minerals in the chalcophile trace elements nickel and copper occurs in the SMB as a result of their incorporation into either the immiscible sulfide melts or *iss*, which crystallize pyrite, pyrrhotite, and chalcopyrite.

5.2 Recommendations for future work

The study of sulfide minerals associated with igneous intrusions is far from complete. Through the use of $\delta^{34}S$ studies, authors such as Poulson, Kubilius, and Ohmoto have proposed models of assimilation of sulfide minerals from sulfide-rich

country-rock; however, their models do not fully explain sulfide interactions in an igneous intrusion such as the SMB. As a result of time constraints, further analysis of $\delta^{34}S$ variations was not possible in this thesis. Study of sulfur isotope variations is necessary in order to fully understand the country-rock magma interactions observed in the SMB.

The occurrence of immiscible sulfide melts in felsic magmas is a subject that also deserves further investigation. In particular, high temperature studies of phase relationships in the Cu-Fe-S system are necessary: i) to explain the presence of immiscible sulfide liquids; ii) to determine the temperature and pressure conditions required for the formation if such liquids; and iii) to work out the detailed crystallization history of the sulfide blebs in the SMB.

References

Amcoff, O. 1981. Heating experiments of chalcopyrite-pyrrhotite ores: studies on the stabilities of intermediate solid solution. Neues Jahrbuch fuer Mineralogie, **1981:** 553-568.

Arndt, N.T., Hallot, H., and de Bremond d'Ars, J. 2001. Analog experimental insights into the formation of magmatic sulfide deposits. Earth and Planetary Science Letters, **186:** 371-381.

Arnold, R.G. 1962. Equilibrium relationships between pyrite and pyrrhotite from 325 ° to 743 °C. Economic Geology, **57:** 72-90.

Bhatnagar, P., Horne, R., and Culshaw, N. 1998. The interplay of regional structure and emplacement mechanisms at the contact of the South Mountain Batholith, Nova Scotia: floor-down or wall-up? Canadian Journal of Earth Sciences, **38:** 1285-1299.

Borrok, D., Kessler, S.E., and Vogel, T.A. 1999. Sulfide minerals in intrusive and volcanic rocks of the Bingham-Park City Belt, Utah. Economic Geology, **94:** 1213-1230.

Cabri, L.J. 1973. New data on phase relations in the Cu-Fe-S system. Economic Geology, **68:** 443-454.

Clarke, D.B. and Chatterjee, A.K. 1988. Physical and chemical processes in the South Mountain Batholith, Nova Scotia. In: Special Volume - Canadian Institute of Mining and Metallurgy, vol.39, pp.223-233.

Clarke, D.B. and Halliday, A.N. 1980. Strontium isotope geology of the South Mountain Batholith, Nova Scotia. Geochimica et Cosmochimica Acta, **44:** 1045-1058.

Clarke, D.B., MacDonald, M.A., Erdmann, S. 2004. Chemical variation in Al (sub 2) O (sub 3) -CaO-Na (sub 2) O-K (sub 2) O space; controls on the peraluminosity of the South Mountain Batholith. Canadian Journal of Earth Sciences, **41:** 785-798.

Clarke, D.B. and Muecke, G.K. 1985. Review of the petrochemistry and origin of the South Mountain Batholith and associated plutons, Nova Scotia, Canada. In: The Institute of Mining and High Heat Production Granites, Hydrothermal Ore Genesis. Canadian Institute of Mining and Metallurgy, Montreal, Que., pp. 41-54.

Craig, J.R., Vokes, F.M., and Solberg, T.N. 1998. Pyrite: physical and chemical textures, Mineralium Deposita, **34:** 82-101.

Desborough, G.A. and Carpenter, R.H. 1965. Phase relations of pyrrhotite. Economic Geology, **60:** 1431-1450.

Faribault, E.R. 1914. Geology of the Port Mouton map area, Queens County, N. S; Summary Report of the Geological Survey of Canada, pp.251-258.

Fox, D., Robinson, C., and Zentilli, M. 1997. Pyrrhotite and associated sulphides and their relationship to acid rock drainage in the Halifax Formation, Meguma Group, Nova Scotia. Atlantic Geology, **33**: 87-103.

Ghosh-Dastidar, P., Pajari, G.E., and Trembath, L.T. 1970. Factors affecting the trace element partition coefficients between coexisting sulfides. Economic Geology, **65**: 815-837.

Graves, M.C. and Zentilli, M. 1988. The lithochemistry of metal-enriched coticules in the Goldenville-Halifax transition zone of the Meguma Group, Nova Scotia. Paper - Geological Survey of Canada, **88 1-B**: 251-261.

Ham, L.J., Corey, M.C., Horne, R.J., and MacDonald, M.A. 1990. Lithogeochemistry of the western portion of the South Mountain Batholith, Nova Scotia. Nova Scotia Department of Mines and Energy, Open File Report 90-007.

Harris, I.M. and Schenk, P.E. 1975. The Meguma Group. Maritime Sediments, **11**: 25-46.

Hawley, J.E. and Nichol, I. 1961. Trace elements in pyrite, pyrrhotite and chalcopyrite of different ores. Economic Geology, **56**: 467-484.

Huston, D.L., Suter, G.F., Sie, S.H., Cooke, D.R., and Both, R.A. 1995. Trace elements in sulfide minerals from Eastern Australian volcanic-hosted massive sulfide deposits: Part I. Proton microprobe analysis of pyrite, chalcopyrite, and sphalerite, and Part II. Selenium levels in pyrite: Comparison with $\delta^{34}S$ values and implications for the source of sulfur in volcanogenic hydrothermal systems. Economic Geology, **90**: 1167-1198.

Imai, A. 1994. Sulfide globules associated with a felsite intrusion in the Mount Kinabalu quartz monzogranite, Sabah, East Malaysia: Sulfide melt immiscibility in a highly silicic melt. Economic Geology, **89**: 181-185.

Jamieson, R.A. 1974. The contact of the South Mountain Batholith near Mount Uniacke, Nova Scoita. B.Sc. thesis, Dalhousie University, Halifax, N.S.

Koster van Gross, A.F. 1967. The origin of sulfide deposits : Petrographic evidence for liquid immiscibility between silicate magmas and sulfide melts. Economic Geology, **62**: 551-561.

Lusk, J. and Bray, D.M. 2002. Phase relations and the electrochemical determination of sulfur fugacity for selected reactions in the Cu-Fe-S and Fe-S systems at 1 bar and temperatures between 185-460 ° C. Chemical Geology, **192**: 227-248.

Macdonald, M.C., Horne, R.J., Corey, M.C., and Ham, L.J. 1992. Structure and emplacement of the South Mountain Batholith, southwestern Nova Scotia. Atlantic Geology, **28:** 29-50.

Nesse, W.D. 2000. Introduction to Mineralogy. Oxford University Press. New York.

Phinney, W.C. 1961. Possible turbidity-current deposit in Nova Scotia. Geological Society of America Bulletin, **72:** 1453-1454.

Poulson, S.R., Kubilius, W.P., and Ohmoto, H. 1991. Goechemical behavior of sulfur in granitoids during intrusion of the South Mountain Batholith, Nova Scotia, Canada. Geochemica et Cosmochimica Acta, **55:** 3809-3830.

Powell, W.G. and Pattison, D.R.M. 1997. An exsolution origin for low-temperature sulfides at the Hemlo gold deposit, Ontario, Canada. Economic Geology, **92:** 569-577.

Ramdohr, P. 1980. The Ore Minerals and their Intergrowths. Permagon Press. Berlin.

Schenk, P.E. 1997. Sequence stratigraphy and provenance on Gondwana's margin: The Meguma Zone (Cambrian to Devonian) of Nova Scotia, Canada. Geological Society of America, **109:** 395-409.

Smyth, P.K. and Kontak, D.J. 1988. The emergence of a major, turbidite-hosted gold province in the lower Palaeozoic Meguma Group, Nova Scotia, Canada. Abstracts - Geological Society of Australia, **23:** 224-226.

Taylor, F.C. and Schiller, E.A. 1966. Metamorphism of the Meguma group of Nova Scotia. Canadian Journal of Earth Sciences, **3:** 959-974.

Tomkins, A.G. and Mavrogens, J.A. 2003. Generation of metal-rich felsic magmas during crustal anatexis. Geology, **31:** 765-768.

Yund, R.A. and Hall, H.T. 1970. Kinetics of Pyrite exsolution from pyrrhotite. Journal of Petrology, **11:** 381-404.

Yund, R.A. and Kullerud, G. 1966. Thermal stability of assemblages in Cu-Fe-S system. Journal of Petrology, **7:** 454-488.

Appendix A

Mass Percent   Structural Formula

No.	S	Fe	As	Ni	Pb	Cu	Zn	Total	Sample #	Mineral	Location	Fe	Cu	S	Ni	As
138	34.75	31.19	0.00	0.00	0.04	33.90	0.07	99.95	6860-1	cpy	meguma	1.031	0.985	2.000	0.000	0.000
139	35.22	31.43	0.00	0.00	0.00	33.51	0.03	100.18	6860-2	cpy	meguma	1.025	0.960	2.000	0.000	0.000
141	34.97	31.80	0.00	0.00	0.01	33.64	0.02	100.44	6859-1	cpy	meguma	1.044	0.971	2.000	0.000	0.000
149	34.94	31.37	0.00	0.00	0.03	33.97	0.07	100.38	6852-1	cpy	meguma	1.031	0.981	2.000	0.000	0.000
153	34.92	31.25	0.00	0.00	0.05	33.99	0.05	100.26	6856-1	cpy	meguma	1.027	0.982	2.000	0.000	0.000
155	34.92	31.31	0.00	0.01	0.07	33.75	0.09	100.15	6854-1	cpy	meguma	1.030	0.975	2.000	0.000	0.000
157	34.69	31.44	0.02	0.00	0.11	33.27	0.08	99.61	6854-3	cpy	meguma	1.041	0.968	2.000	0.000	0.000
162	34.87	31.83	0.00	0.00	0.09	33.68	0.04	100.50	6823-1	cpy	meguma	1.048	0.975	2.000	0.000	0.000
164	34.92	31.99	0.00	0.00	0.00	33.42	0.06	100.39	6824-1	cpy	meguma	1.052	0.966	2.000	0.000	0.000
198	34.90	31.93	0.00	0.00	0.00	33.74	0.01	100.58	6839-1	cpy	meguma	1.051	0.976	2.000	0.000	0.000
202	35.26	31.44	0.00	0.00	0.00	34.12	0.00	100.82	6841-1	cpy	meguma	1.024	0.977	2.000	0.000	0.000
278	34.98	31.08	0.00	0.00	0.00	33.44	0.10	99.60	6921-1	cpy	meguma	1.021	0.965	2.000	0.000	0.000
279	34.96	31.40	0.00	0.00	0.00	33.39	0.05	99.81	6921-2	cpy	meguma	1.031	0.964	2.000	0.000	0.000
118	34.51	30.63	0.00	0.00	0.05	32.19	0.03	97.40	6846-1	cpy	meguma	1.019	0.941	2.000	0.000	0.000
129	34.64	30.80	0.00	0.03	0.00	33.14	0.02	98.63	6843-1	cpy	meguma	1.021	0.966	2.000	0.001	0.000
130	34.21	31.02	0.00	0.00	0.08	33.16	0.03	98.50	6843-2	cpy	meguma	1.041	0.978	2.000	0.000	0.000
136	35.00	31.19	0.01	0.00	0.05	33.62	0.02	99.89	6849-3	cpy	meguma	1.023	0.969	2.000	0.000	0.000
173	35.19	31.85	0.00	0.00	0.00	33.85	0.04	100.93	6819-1	cpy	meguma	1.039	0.971	2.000	0.000	0.000
175	35.00	31.61	0.02	0.00	0.00	33.42	0.01	100.06	6818-1	cpy	meguma	1.037	0.964	2.000	0.000	0.000
176	35.27	31.62	0.00	0.01	0.00	33.98	0.13	101.01	6818-2	cpy	meguma	1.029	0.972	2.000	0.000	0.000
52	35.59	30.80	0.00	0.00	0.05	34.95	0.00	101.39	6644-1	cpy	meguma	0.994	0.991	2.000	0.000	0.000
55	35.12	30.30	0.00	0.00	0.00	34.82	0.09	100.33	6657-1	cpy	meguma	0.991	1.001	2.000	0.000	0.000
61	35.64	29.63	0.00	0.00	0.02	34.68	0.08	100.06	6658-1	cpy	meguma	0.955	0.982	2.000	0.000	0.000
134	35.14	30.99	0.00	0.01	0.05	34.07	0.04	100.31	6849-1	cpy	meguma	1.013	0.979	2.000	0.000	0.000
average	34.98	31.25	0.00	0.00	0.03	33.74	0.05	100.05				1.026	0.973	2.000	0.000	0.000
std dev	0.31	0.55	0.01	0.01	0.03	0.58	0.03									
196	45.09	53.74	0.01	0.11	0.00	0.01	0.03	98.99	6838-2	mix	meguma	1.368	0.000	2.000	0.003	0.000
197	44.37	55.50	0.00	0.09	0.00	0.00	0.00	99.95	6838-3	mix	meguma	1.436	0.000	2.000	0.002	0.000
204	47.58	52.21	0.00	0.11	0.00	0.09	0.00	99.99	6841-3	mix	meguma	1.260	0.002	2.000	0.003	0.000
60	43.75	52.90	0.00	0.25	0.07	0.02	0.01	97.00	6656-3	mix	meguma	1.388	0.001	2.000	0.006	0.000
57	47.48	50.06	0.00	0.13	0.01	0.00	0.00	97.69	6657-3	mix	meguma	1.211	0.000	2.000	0.003	0.000

291	50.02	48.85	0.00	0.15	0.00	0.00	0.01	99.03	6658-1	mix	meguma	1.121	0.000	2.000	0.003	0.000
292	50.78	46.88	0.00	0.10	0.00	0.02	0.00	97.78	6658-2	mix	meguma	1.060	0.000	2.000	0.002	0.000
295	47.98	49.94	0.00	0.16	0.03	0.03	0.00	98.16	6658-5	mix	meguma	1.195	0.001	2.000	0.004	0.000
296	44.74	50.58	0.00	0.24	0.00	0.00	0.00	95.56	6656-1	mix	meguma	1.298	0.000	2.000	0.006	0.000
297	46.11	50.73	0.00	0.25	0.00	0.08	0.00	97.17	6656-2	mix	meguma	1.263	0.002	2.000	0.006	0.000
298	49.57	47.09	0.00	0.28	0.00	0.01	0.00	96.96	6656-3	mix	meguma	1.091	0.000	2.000	0.006	0.000
299	41.48	49.81	0.00	0.22	0.00	0.00	0.04	91.56	6656-4	mix	meguma	1.379	0.000	2.000	0.006	0.000
average	46.58	50.69	0.00	0.18	0.01	0.02	0.01	97.49				1.250	0.000	2.000	0.004	0.000
std dev	2.81	2.56	0.00	0.07	0.02	0.03	0.01									
65	53.72	46.52	0.32	0.04	0.05	0.03	0.01	100.68	6659-1	py	meguma	0.994	0.001	2.000	0.001	0.005
142	52.67	48.16	0.00	0.15	0.00	0.03	0.00	101.02	6859-2	py	meguma	1.050	0.001	2.000	0.003	0.000
144	52.87	45.25	0.05	0.12	0.00	0.59	0.04	98.91	6858-1	py	meguma	0.983	0.011	2.000	0.003	0.001
146	51.82	45.66	0.00	0.13	0.00	0.00	0.00	97.61	6858-3	py	meguma	1.012	0.000	2.000	0.003	0.000
154	52.82	48.26	0.00	0.05	0.00	0.00	0.02	101.16	6856-2	py	meguma	1.049	0.000	2.000	0.001	0.000
156	52.86	47.86	0.00	0.05	0.00	0.05	0.03	100.84	6854-2	py	meguma	1.040	0.001	2.000	0.001	0.000
158	52.89	48.07	0.00	0.07	0.06	0.04	0.06	101.19	6854-4	py	meguma	1.044	0.001	2.000	0.001	0.000
166	52.93	48.20	0.00	0.01	0.02	0.02	0.00	101.19	6825-1	py	meguma	1.046	0.000	2.000	0.000	0.000
167	53.42	48.26	0.00	0.00	0.00	0.00	0.00	101.69	6825-2	py	meguma	1.037	0.000	2.000	0.000	0.000
168	52.91	47.92	0.00	0.00	0.09	0.00	0.00	100.92	6825-3	py	meguma	1.040	0.000	2.000	0.000	0.000
159	53.35	48.14	0.01	0.08	0.02	0.00	0.00	101.60	6855-1	py	meguma	1.036	0.000	2.000	0.002	0.000
160	53.17	47.91	0.00	0.00	0.04	0.00	0.04	101.17	6855-2	py	meguma	1.035	0.000	2.000	0.000	0.000
161	53.27	47.87	0.00	0.00	0.01	0.05	0.00	101.19	6855-3	py	meguma	1.032	0.001	2.000	0.000	0.000
184	54.26	48.31	0.00	0.06	0.00	0.06	0.00	102.69	6831-1	py	meguma	1.022	0.001	2.000	0.001	0.000
185	52.11	43.77	0.01	1.98	0.08	0.01	0.00	97.96	6831-2	py	meguma	0.965	0.000	2.000	0.042	0.000
190	54.01	47.71	0.00	0.01	0.06	0.01	0.03	101.83	6822-1	py	meguma	1.014	0.000	2.000	0.000	0.000
205	53.39	48.08	0.00	0.09	0.08	0.00	0.04	101.67	6827-1	py	meguma	1.034	0.000	2.000	0.002	0.000
186	54.38	48.37	0.00	0.00	0.03	0.08	0.07	102.91	6830-1	py	meguma	1.021	0.001	2.000	0.000	0.000
187	54.26	48.54	0.00	0.00	0.00	0.00	0.00	102.80	6830-2	py	meguma	1.027	0.000	2.000	0.000	0.000
188	54.11	47.92	0.00	0.00	0.00	0.00	0.01	102.04	6832-1	py	meguma	1.017	0.000	2.000	0.000	0.000
189	54.21	47.86	0.00	0.00	0.00	0.00	0.00	102.08	6832-2	py	meguma	1.014	0.000	2.000	0.000	0.000
191	54.12	48.13	0.00	0.04	0.00	0.04	0.04	102.37	6821-1	py	meguma	1.021	0.001	2.000	0.001	0.000
192	54.34	48.28	0.02	0.02	0.00	0.02	0.00	102.67	6821-2	py	meguma	1.020	0.000	2.000	0.000	0.000
193	54.25	48.39	0.00	0.00	0.00	0.00	0.00	102.64	6820-1	py	meguma	1.024	0.000	2.000	0.000	0.000
194	54.47	48.57	0.00	0.00	0.00	0.03	0.01	103.09	6820-2	py	meguma	1.024	0.001	2.000	0.000	0.000
45	53.80	47.20	0.02	0.13	0.00	0.00	0.00	101.15	6642-1	py	meguma	1.008	0.000	2.000	0.003	0.000
47	53.98	46.45	0.02	0.10	0.00	0.00	0.04	100.59	6643-1	py	meguma	0.988	0.000	2.000	0.002	0.000

49	53.59	47.51	0.00	0.06	0.00	0.05	0.05	101.26	6645-1	py	meguma	1.018	0.001	2.000	0.001	0.000
125	51.58	46.66	0.00	0.10	0.00	0.02	0.01	98.36	6844-1	py	meguma	1.039	0.000	2.000	0.002	0.000
180	52.77	47.15	0.05	0.11	0.00	0.06	0.00	100.13	6816-3	py	meguma	1.026	0.001	2.000	0.002	0.001
111	51.46	45.98	0.01	0.15	0.00	0.01	0.02	97.62	6648-1	py	meguma	1.026	0.000	2.000	0.003	0.000
112	51.49	46.74	0.00	0.11	0.00	0.02	0.02	98.39	6848-2	py	meguma	1.042	0.000	2.000	0.002	0.000
115	51.74	45.67	0.00	0.15	0.00	0.00	0.04	97.60	6847-2	py	meguma	1.014	0.000	2.000	0.003	0.000
117	51.67	46.45	0.02	0.16	0.08	0.03	0.00	98.41	6848-4	py	meguma	1.032	0.001	2.000	0.003	0.000
178	53.22	47.05	0.00	0.13	0.00	0.00	0.01	100.41	6816-1	py	meguma	1.015	0.000	2.000	0.003	0.000
183	53.25	47.40	0.01	0.13	0.00	0.00	0.05	100.84	6815-2	py	meguma	1.022	0.000	2.000	0.003	0.000
average	53.20	47.40	0.02	0.12	0.02	0.03	0.02	100.80				1.023	0.001	2.000	0.002	0.000
std dev	0.92	1.10	0.05	0.32	0.03	0.10	0.02									
143	39.94	60.55	0.00	0.05	0.00	0.04	0.00	100.57	6859-3	pyrr	meguma	0.870	0.001	1.000	0.001	0.000
148	41.26	58.39	0.01	0.12	0.00	0.00	0.03	99.81	6857-2	pyrr	meguma	0.813	0.000	1.000	0.002	0.000
140	39.66	60.91	0.00	0.02	0.02	0.00	0.03	100.66	6860-3	pyrr	meguma	0.882	0.000	1.000	0.000	0.000
150	39.68	61.19	0.00	0.14	0.00	0.00	0.01	101.02	6852-2	pyrr	meguma	0.885	0.000	1.000	0.002	0.000
152	39.57	59.80	0.00	0.15	0.00	0.00	0.00	99.53	6852-4	pyrr	meguma	0.868	0.000	1.000	0.002	0.000
163	38.85	62.04	0.00	0.00	0.00	0.01	0.00	100.90	6823-2	pyrr	meguma	0.917	0.000	1.000	0.000	0.000
165	39.18	61.81	0.00	0.04	0.00	0.00	0.00	101.03	6824-2	pyrr	meguma	0.906	0.000	1.000	0.001	0.000
147	39.74	60.15	0.00	0.00	0.01	0.00	0.02	99.91	6857-1	pyrr	meguma	0.869	0.000	1.000	0.000	0.000
195	38.85	62.64	0.00	0.04	0.00	0.06	0.01	101.60	6838-1	pyrr	meguma	0.926	0.001	1.000	0.001	0.000
199	39.11	61.43	0.00	0.10	0.00	0.02	0.01	100.66	6839-2	pyrr	meguma	0.902	0.000	1.000	0.001	0.000
200	38.94	61.69	0.01	0.11	0.01	0.02	0.00	100.77	6840-1	pyrr	meguma	0.910	0.000	1.000	0.001	0.000
203	38.99	61.69	0.00	0.06	0.05	0.00	0.00	100.79	6841-2	pyrr	meguma	0.909	0.000	1.000	0.001	0.000
206	39.81	60.94	0.00	0.03	0.02	0.00	0.00	100.80	6827-2	pyrr	meguma	0.879	0.000	1.000	0.000	0.000
207	39.12	61.58	0.00	0.11	0.14	0.02	0.00	100.97	6829-1	pyrr	meguma	0.904	0.000	1.000	0.002	0.000
280	38.54	61.12	0.00	0.09	0.02	0.07	0.00	99.84	6921-3	pyrr	meguma	0.911	0.001	1.000	0.001	0.000
281	39.18	60.72	0.00	0.11	0.01	0.00	0.00	100.03	6930-1	pyrr	meguma	0.890	0.000	1.000	0.001	0.000
282	38.99	60.50	0.00	0.11	0.06	0.01	0.00	99.66	6930-2	pyrr	meguma	0.891	0.000	1.000	0.002	0.000
283	39.72	60.76	0.00	0.10	0.00	0.04	0.00	100.62	6930-3	pyrr	meguma	0.878	0.001	1.000	0.001	0.000
284	38.95	60.24	0.00	0.11	0.00	0.04	0.01	99.36	6930-4	pyrr	meguma	0.888	0.001	1.000	0.002	0.000
51	39.16	60.70	0.00	0.04	0.00	0.03	0.05	99.98	6645-3	pyrr	meguma	0.890	0.000	1.000	0.001	0.000
46	38.96	60.38	0.02	0.07	0.00	0.02	0.03	99.48	6642-2	pyrr	meguma	0.890	0.000	1.000	0.001	0.000
48	39.24	59.48	0.00	0.11	0.00	0.01	0.00	98.84	6643-2	pyrr	meguma	0.870	0.000	1.000	0.002	0.000
53	39.01	60.21	0.00	0.08	0.02	0.11	0.00	99.42	6644-2	pyrr	meguma	0.886	0.001	1.000	0.001	0.000
54	38.97	60.33	0.00	0.05	0.00	0.02	0.00	99.38	6644-3	pyrr	meguma	0.889	0.000	1.000	0.001	0.000
56	39.23	59.87	0.00	0.12	0.00	0.09	0.01	99.31	6657-2	pyrr	meguma	0.876	0.001	1.000	0.002	0.000

58	39.15	58.89	0.00	0.19	0.00	0.00	0.01	98.24	6656-1	pyrr	meguma	0.864	0.000	1.000	0.003	0.000
59	39.65	58.86	0.00	0.15	0.00	0.01	0.00	98.68	6656-2	pyrr	meguma	0.852	0.000	1.000	0.002	0.000
62	40.36	58.63	0.00	0.09	0.00	0.09	0.02	99.19	6658-2	pyrr	meguma	0.834	0.001	1.000	0.001	0.000
63	40.30	58.02	0.00	0.08	0.06	0.11	0.03	98.60	6658-3	pyrr	meguma	0.827	0.001	1.000	0.001	0.000
113	38.88	59.16	0.00	0.24	0.00	0.00	0.04	98.32	6848-3	pyrr	meguma	0.874	0.000	1.000	0.003	0.000
114	38.53	59.10	0.01	0.03	0.00	0.01	0.02	97.70	6847-1	pyrr	meguma	0.881	0.000	1.000	0.000	0.000
116	38.35	59.39	0.00	0.05	0.00	0.02	0.02	97.84	6848-3	pyrr	meguma	0.889	0.000	1.000	0.001	0.000
119	38.45	59.76	0.00	0.14	0.00	0.04	0.03	98.42	6846-2	pyrr	meguma	0.892	0.000	1.000	0.002	0.000
120	38.23	60.11	0.00	0.14	0.07	0.04	0.00	98.57	6846-3	pyrr	meguma	0.903	0.000	1.000	0.002	0.000
123	38.68	60.03	0.02	0.12	0.00	0.05	0.02	98.91	6845-3	pyrr	meguma	0.891	0.001	1.000	0.002	0.000
124	39.14	59.65	0.03	0.08	0.13	0.01	0.00	99.05	6845-4	pyrr	meguma	0.875	0.000	1.000	0.001	0.000
128	38.47	59.11	0.00	0.14	0.07	0.00	0.01	97.80	6842-2	pyrr	meguma	0.882	0.000	1.000	0.002	0.000
131	38.34	60.14	0.01	0.09	0.00	0.00	0.03	98.61	6843-3	pyrr	meguma	0.901	0.000	1.000	0.001	0.000
133	39.04	61.01	0.00	0.02	0.00	0.03	0.00	100.10	6851-2	pyrr	meguma	0.897	0.000	1.000	0.000	0.000
135	38.85	61.38	0.00	0.16	0.00	0.04	0.01	100.43	6849-2	pyrr	meguma	0.907	0.000	1.000	0.002	0.000
177	39.48	61.48	0.00	0.13	0.00	0.00	0.01	101.11	6818-3	pyrr	meguma	0.894	0.000	1.000	0.002	0.000
64	39.29	59.37	0.00	0.16	0.00	0.05	0.01	98.87	6658-4	pyrr	meguma	0.868	0.001	1.000	0.002	0.000
174	39.68	60.76	0.00	0.28	0.00	0.05	0.05	100.82	6819-2	pyrr	meguma	0.879	0.001	1.000	0.004	0.000
289	39.07	60.91	0.00	0.05	0.02	0.01	0.00	100.06	6922-2	pyrr	meguma	0.895	0.000	1.000	0.001	0.000
293	39.16	61.11	0.00	0.12	0.00	0.02	0.03	100.43	6658-3	pyrr	meguma	0.896	0.000	1.000	0.002	0.000
294	39.05	61.32	0.00	0.12	0.00	0.05	0.00	100.54	6658-4	pyrr	meguma	0.902	0.001	1.000	0.002	0.000
300	38.97	60.49	0.00	0.18	0.00	0.00	0.00	99.64	6656-5	pyrr	meguma	0.891	0.000	1.000	0.003	0.000
301	38.90	60.60	0.00	0.19	0.00	0.01	0.02	99.73	6656-6	pyrr	meguma	0.895	0.000	1.000	0.003	0.000
average	39.18	60.38	0.00	0.10	0.01	0.03	0.01	99.72				0.885	0.000	1.000	0.001	0.000
std dev	0.57	1.02	0.01	0.06	0.03	0.03	0.01									
89	35.61	30.36	0.00	0.00	0.03	34.03	0.76	100.80	6649-3	cpy	SMB	0.979	0.965	2.000	0.000	0.000
92	35.27	30.22	0.00	0.00	0.04	34.44	0.83	100.81	6648-2	cpy	SMB	0.984	0.985	2.000	0.000	0.000
21	35.21	29.99	0.03	0.00	0.08	34.26	0.02	99.60	cpy D-663	cpy	SMB	0.978	0.982	2.000	0.000	0.001
23	35.05	30.50	0.00	0.00	0.07	34.21	0.04	99.88	cpy D-663	cpy	SMB	0.999	0.985	2.000	0.000	0.000
101	35.59	30.94	0.02	0.01	0.00	34.07	0.07	100.70	6666-1	cpy	SMB	0.998	0.966	2.000	0.000	0.000
13	35.09	30.32	0.00	0.00	0.08	33.55	0.00	99.05	cpy E-663	cpy	SMB	0.992	0.965	2.000	0.000	0.000
15	34.92	30.29	0.00	0.00	0.08	33.33	0.00	98.62	cpy E-663	cpy	SMB	0.996	0.963	2.000	0.000	0.000
34	34.89	30.60	0.00	0.00	0.01	34.86	0.09	100.44	cpy B-663	cpy	SMB	1.007	1.008	2.000	0.000	0.000
35	35.30	30.77	0.00	0.00	0.07	34.78	0.09	101.00	cpy B-663	cpy	SMB	1.001	0.994	2.000	0.000	0.000
37	34.87	30.49	0.03	0.00	0.00	34.51	0.08	99.98	cpy B-662	cpy	SMB	1.004	0.999	2.000	0.000	0.001

39	35.77	30.44	0.00	0.00	0.12	34.62	0.11	101.07	cpy B-663	cpy	SMB	0.977	0.977	2.000	0.000	0.000
40	34.79	30.54	0.00	0.00	0.05	34.85	0.04	100.28	cpy B-663	cpy	SMB	1.008	1.011	2.000	0.000	0.000
98	35.78	30.44	0.00	0.00	0.00	34.90	0.04	101.16	6654-3	cpy	SMB	0.977	0.984	2.000	0.000	0.000
4	35.00	30.52	0.00	0.00	0.06	34.76	0.00	100.34	cpy A-663	cpy	SMB	1.001	1.002	2.000	0.000	0.000
5	34.85	30.76	0.00	0.01	0.05	34.94	0.00	100.60	cpy A-663	cpy	SMB	1.014	1.012	2.000	0.000	0.000
7	35.72	31.52	0.00	0.02	0.07	33.49	0.00	100.82	cpy A-663	cpy	SMB	1.013	0.946	2.000	0.001	0.000
11	34.98	30.72	0.00	0.00	0.00	35.17	0.00	100.87	PY E-6639	cpy	SMB	1.008	1.015	2.000	0.000	0.000
29	34.35	30.44	0.00	0.00	0.11	35.19	0.02	101.11	cpy F-662	cpy	SMB	1.018	1.034	2.000	0.000	0.000
95	35.44	30.73	0.01	0.00	0.25	34.98	0.09	101.51	6651-2	cpy	SMB	0.996	0.996	2.000	0.000	0.000
99	35.55	30.79	0.00	0.00	0.00	34.80	0.09	101.22	6650-1	cpy	SMB	0.995	0.988	2.000	0.000	0.000
104	35.37	30.35	0.00	0.00	0.00	34.66	0.07	100.45	6665-1	cpy	SMB	0.985	0.989	2.000	0.000	0.000
105	34.98	30.01	0.00	0.00	0.00	34.91	0.10	100.00	6665-2	cpy	SMB	0.985	1.007	2.000	0.000	0.000
253	34.88	30.45	0.00	0.00	0.00	34.01	0.04	99.38	6916-1	cpy	SMB	1.003	0.984	2.000	0.000	0.000
254	34.77	30.61	0.00	0.01	0.00	33.57	0.13	99.08	6916-2	cpy	SMB	1.011	0.974	2.000	0.000	0.000
average	35.17	30.53	0.00	0.00	0.05	34.45	0.11	100.37				0.997	0.989	2.000	0.000	0.000
std dev	0.37	0.31	0.01	0.01	0.06	0.56	0.21									Zn
96	34.51	9.66	0.00	0.02	0.00	2.15	56.74	103.07	6654-1	sphalerit	SMB	0.161	0.031	1.000	0.000	1.613
average	34.51	9.66	0.00	0.02	0.00	2.15	56.74	103.07				0.161	0.031	1.000	0.000	1.613
																As
12	52.32	44.50	2.11	0.56	0.00	1.02	0.00	100.51	PY E-6638	py	SMB	0.977	0.020	2.000	0.012	0.035
14	53.72	47.02	0.00	0.05	0.00	0.13	0.00	100.92	PY E-6630	py	SMB	1.005	0.002	2.000	0.001	0.000
33	53.34	47.12	0.00	0.21	0.10	0.42	0.00	101.20	PY B-6636	py	SMB	1.014	0.008	2.000	0.004	0.000
36	54.02	46.92	0.00	0.17	0.09	0.18	0.04	101.41	PY B-6629	py	SMB	0.998	0.003	2.000	0.003	0.000
6	52.96	47.44	0.03	0.02	0.00	0.00	0.00	100.44	PY A-6631	py	SMB	1.029	0.000	2.000	0.000	0.001
8	53.34	47.28	0.00	0.30	0.00	0.01	0.00	100.93	PY A-6631	py	SMB	1.018	0.000	2.000	0.006	0.000
9	53.37	46.54	0.00	0.00	0.03	0.00	0.00	99.95	PY A-6633	py	SMB	1.001	0.000	2.000	0.000	0.000
22	53.11	46.87	0.00	0.59	0.00	0.13	0.02	100.72	PY D-6637	py	SMB	1.013	0.003	2.000	0.012	0.000
24	52.85	45.94	0.00	0.25	0.10	0.32	0.02	99.49	PY D-6637	py	SMB	0.998	0.006	2.000	0.005	0.000
27	53.29	47.11	0.00	0.05	0.12	0.00	0.03	100.60	PY C-6625	py	SMB	1.015	0.000	2.000	0.001	0.000
28	52.81	47.44	0.00	0.14	0.18	0.04	0.04	100.65	PY C-6625	py	SMB	1.032	0.001	2.000	0.003	0.000
30	51.80	45.88	0.00	0.00	0.06	0.01	0.00	97.75	PY F-6628	py	SMB	1.017	0.000	2.000	0.000	0.000
31	51.71	45.42	0.00	0.02	0.00	0.13	0.00	97.28	PY F-6628	py	SMB	1.009	0.003	2.000	0.000	0.000
32	53.77	46.82	0.00	0.66	0.06	0.01	0.00	101.33	PY B-6636	py	SMB	1.000	0.000	2.000	0.013	0.000
38	53.94	47.27	0.00	0.15	0.00	0.02	0.00	101.37	PY B-6635	py	SMB	1.006	0.000	2.000	0.003	0.000
10	53.33	47.20	0.15	0.70	0.00	0.03	0.00	101.41	PY E-6639	py	SMB	1.016	0.001	2.000	0.014	0.002
245	53.43	45.69	0.00	0.75	0.00	0.06	0.00	99.94	6914-1	py	SMB	0.982	0.001	2.000	0.015	0.000

246	53.78	46.50	0.01	0.33	0.00	0.02	0.00	100.64	6914-2	py	SMB	0.993	0.000	2.000	0.007	0.000
247	53.63	43.24	0.00	4.19	0.00	0.02	0.00	101.08	6914-3	py	SMB	0.926	0.000	2.000	0.085	0.000
250	53.51	46.10	0.00	0.64	0.00	0.01	0.00	100.25	6915-1	py	SMB	0.989	0.000	2.000	0.013	0.000
251	53.01	45.27	0.00	1.32	0.00	0.67	0.00	100.27	6915-2	py	SMB	0.981	0.013	2.000	0.027	0.000
average	53.19	46.36	0.11	0.53	0.04	0.15	0.01	100.39				1.001	0.003	2.000	0.011	0.002
std dev	0.63	1.08	0.46	0.90	0.05	0.26	0.01									
66	39.43	58.63	0.00	0.09	0.19	0.00	0.06	98.40	6647-1	pyrr	SMB	0.854	0.000	1.000	0.001	0.000
93	39.07	60.60	0.00	0.19	0.00	0.09	0.00	99.95	6648-3	pyrr	SMB	1.781	0.002	2.000	0.005	0.000
88	40.08	60.34	0.00	0.07	0.00	0.05	0.00	100.54	6649-2	pyrr	SMB	1.729	0.001	2.000	0.002	0.000
86	40.22	59.71	0.00	0.34	0.08	0.04	0.03	100.42	6646-1	pyrr	SMB	1.705	0.001	2.000	0.009	0.000
94	39.55	59.87	0.00	0.27	0.06	0.17	0.00	99.92	6651-1	pyrr	SMB	1.739	0.004	2.000	0.008	0.000
97	39.51	60.64	0.00	0.22	0.04	0.24	0.06	100.71	6654-2	pyrr	SMB	1.762	0.006	2.000	0.006	0.000
100	39.49	60.49	0.02	0.26	0.00	0.04	0.02	100.32	6650-2	pyrr	SMB	1.759	0.001	2.000	0.007	0.000
103	39.14	59.74	0.00	0.24	0.14	0.02	0.00	99.29	6666-3	pyrr	SMB	1.753	0.001	2.000	0.007	0.000
106	38.95	60.69	0.00	0.27	0.01	0.05	0.04	100.00	6665-3	pyrr	SMB	1.789	0.001	2.000	0.007	0.000
248	39.96	59.43	0.00	0.41	0.02	0.04	0.00	99.85	6914-4	pyrr	SMB	1.708	0.001	2.000	0.011	0.000
249	39.68	59.74	0.00	0.30	0.00	0.01	0.00	99.73	6914-5	pyrr	SMB	1.729	0.000	2.000	0.008	0.000
252	39.35	59.69	0.00	0.29	0.03	0.01	0.00	99.37	6915-3	pyrr	SMB	1.742	0.000	2.000	0.008	0.000
255	39.69	60.01	0.00	0.33	0.00	0.00	0.00	100.02	6916-3	pyrr	SMB	1.736	0.000	2.000	0.009	0.000
average	39.55	59.97	0.00	0.25	0.04	0.06	0.02	99.89				1.741	0.001	2.000	0.007	0.000
std dev	0.38	0.59	0.01	0.09	0.06	0.07	0.02									Zn
90	34.13	11.02	0.00	0.00	0.00	0.08	56.32	101.56	6649-4	sphalerit	SMB	0.185	0.001	1.000	0.000	0.000
25	33.73	6.18	0.00	0.01	0.00	3.49	59.73	103.15	??	sphalerit	SMB	0.210	0.105	2.000	0.000	0.000
average	33.93	8.60	0.00	0.01	0.00	1.79	58.03	102.35				0.291	0.053	2.000	0.000	0.000
																As
73	34.58	29.94	0.00	0.00	0.04	35.06	0.06	99.68	6664-3	cpy	xenolith	0.994	1.023	2.000	0.000	0.000
74	35.75	30.46	0.00	0.00	0.00	34.97	0.08	101.27	6663-1	cpy	xenolith	0.978	0.987	2.000	0.000	0.000
75	35.74	30.50	0.00	0.00	0.00	34.89	0.09	101.23	6663-2	cpy	xenolith	0.980	0.985	2.000	0.000	0.000
82	35.69	31.16	0.00	0.00	0.00	34.28	0.05	101.19	6668-1	cpy	xenolith	1.003	0.969	2.000	0.000	0.000
68	34.75	30.11	0.00	0.00	0.07	34.99	0.03	99.94	6660-2	cpy	xenolith	0.995	1.016	2.000	0.000	0.000
233	35.52	30.50	0.00	0.00	0.00	33.96	0.03	100.01	6674-1	cpy	xenolith	0.986	0.965	2.000	0.000	0.000
234	35.26	30.03	0.00	0.00	0.00	33.18	0.06	98.52	6674-2	cpy	xenolith	0.978	0.950	2.000	0.000	0.000
237	35.35	30.89	0.00	0.00	0.00	33.25	0.04	99.53	6920-1	cpy	xenolith	1.004	0.949	2.000	0.000	0.000
238	35.36	30.94	0.00	0.00	0.00	34.00	0.06	100.35	6920-2	cpy	xenolith	1.005	0.971	2.000	0.000	0.000
242	35.26	30.92	0.00	0.00	0.10	33.19	0.02	99.48	6919-1	cpy	xenolith	1.007	0.950	2.000	0.000	0.000

243	35.34	31.31	0.00	0.00	0.00	33.05	0.02	99.72	6919-2	cpy	xenolith	1.017	0.944	2.000	0.000	0.000
256	35.63	30.94	0.00	0.00	0.00	32.70	0.04	99.32	6928-1	cpy	xenolith	0.997	0.926	2.000	0.000	0.000
258	34.98	31.39	0.00	0.01	0.00	33.46	0.05	99.89	6928-3	cpy	xenolith	1.031	0.966	2.000	0.000	0.000
262	34.44	30.75	0.00	0.00	0.09	34.02	0.08	99.39	6927-1	cpy	xenolith	1.025	0.997	2.000	0.000	0.000
266	34.91	30.80	0.00	0.00	0.00	33.39	0.02	99.12	6926-3	cpy	xenolith	1.013	0.965	2.000	0.000	0.000
269	35.34	31.10	0.00	0.00	0.00	33.38	0.07	99.89	6924-1	cpy	xenolith	1.010	0.953	2.000	0.000	0.000
272	34.95	30.71	0.00	0.00	0.09	33.70	0.06	99.51	6924-4	cpy	xenolith	1.009	0.973	2.000	0.000	0.000
average	35.23	30.73	0.00	0.00	0.02	33.85	0.05	99.88				1.002	0.970	2.000	0.000	0.000
std dev	0.40	0.43	0.00	0.00	0.04	0.76	0.02									
80	52.39	47.26	0.00	0.05	0.00	0.03	0.07	99.80	6670-1	py	xenolith	1.036	0.001	2.000	0.001	0.000
84	53.90	47.26	0.00	0.06	0.00	0.00	0.04	101.25	6669-1	py	xenolith	1.007	0.000	2.000	0.001	0.000
259	52.94	47.35	0.00	0.09	0.00	0.00	0.04	100.41	6929-1	py	xenolith	1.027	0.000	2.000	0.002	0.000
260	52.65	47.70	0.12	0.10	0.00	0.00	0.03	100.61	6929-2	py	xenolith	1.040	0.000	2.000	0.002	0.002
264	53.03	47.53	0.00	0.06	0.01	0.01	0.00	100.65	6926-1	py	xenolith	1.029	0.000	2.000	0.001	0.000
267	53.05	47.45	0.00	0.12	0.00	0.00	0.00	100.63	6926-4	py	xenolith	1.027	0.000	2.000	0.002	0.000
276	52.52	47.68	0.00	0.05	0.00	0.00	0.08	100.34	6923-1	py	xenolith	1.042	0.000	2.000	0.001	0.000
average	52.93	47.46	0.02	0.08	0.00	0.01	0.04	100.53				1.030	0.000	2.000	0.002	0.000
std dev	0.50	0.18	0.05	0.03	0.00	0.01	0.03									
81	39.26	60.55	0.03	0.11	0.06	0.00	0.00	100.01	6670-2	pyrr	xenolith	0.886	0.000	1.000	0.002	0.000
69	39.17	60.19	0.01	0.01	0.00	0.02	0.00	99.40	6660-3	pyrr	xenolith	0.882	0.000	1.000	0.000	0.000
70	39.14	60.58	0.00	0.11	0.00	0.00	0.07	99.90	6660-4	pyrr	xenolith	0.889	0.000	1.000	0.002	0.000
71	38.67	60.66	0.00	0.12	0.00	0.02	0.04	99.50	6664-1	pyrr	xenolith	0.901	0.000	1.000	0.002	0.000
72	39.14	58.82	0.00	0.16	0.00	0.16	0.00	98.28	6664-2	pyrr	xenolith	0.863	0.002	1.000	0.002	0.000
83	39.51	60.81	0.02	0.11	0.02	0.05	0.06	100.58	6668-2	pyrr	xenolith	0.884	0.001	1.000	0.002	0.000
85	39.40	60.34	0.01	0.11	0.00	0.00	0.03	99.90	6669-2	pyrr	xenolith	0.879	0.000	1.000	0.002	0.000
235	39.07	60.23	0.00	0.06	0.00	0.07	0.08	99.50	6674-3	pyrr	xenolith	0.885	0.001	1.000	0.001	0.000
236	39.04	60.53	0.00	0.06	0.00	0.23	0.02	99.88	6674-4	pyrr	xenolith	0.890	0.003	1.000	0.001	0.000
240	38.76	60.46	0.00	0.08	0.00	0.00	0.00	99.30	6920-4	pyrr	xenolith	0.896	0.000	1.000	0.001	0.000
241	38.88	60.05	0.00	0.06	0.00	0.00	0.00	98.99	6920-5	pyrr	xenolith	0.887	0.000	1.000	0.001	0.000
244	39.31	60.26	0.00	0.08	0.00	0.02	0.02	99.69	6919-3	pyrr	xenolith	0.880	0.000	1.000	0.001	0.000
257	39.34	60.99	0.00	0.10	0.00	0.03	0.00	100.46	6928-2	pyrr	xenolith	0.890	0.000	1.000	0.001	0.000
261	38.92	61.24	0.00	0.10	0.00	0.00	0.00	100.25	6929-3	pyrr	xenolith	0.904	0.000	1.000	0.001	0.000
263	38.77	60.90	0.00	0.08	0.00	0.03	0.01	99.80	6927-2	pyrr	xenolith	0.902	0.000	1.000	0.001	0.000
265	39.00	61.01	0.00	0.09	0.00	0.01	0.02	100.13	6926-2	pyrr	xenolith	0.898	0.000	1.000	0.001	0.000
268	38.98	61.04	0.00	0.08	0.00	0.01	0.00	100.11	6926-5	pyrr	xenolith	0.899	0.000	1.000	0.001	0.000

270	39.56	60.65	0.00	0.00	0.06	0.15	0.02	100.45	6924-2	pyrr	xenolith	0.880	0.002	1.000	0.000	0.000
271	39.72	60.03	0.00	0.04	0.07	0.24	0.02	100.12	6924-3	pyrr	xenolith	0.868	0.003	1.000	0.001	0.000
274	39.13	60.70	0.00	0.09	0.01	0.03	0.03	99.99	6925-2	pyrr	xenolith	0.891	0.000	1.000	0.001	0.000
275	39.12	60.92	0.00	0.10	0.00	0.03	0.02	100.19	6925-3	pyrr	xenolith	0.894	0.000	1.000	0.001	0.000
277	39.20	60.56	0.00	0.09	0.00	0.00	0.00	99.85	6923-2	pyrr	xenolith	0.887	0.000	1.000	0.001	0.000
average	39.14	60.52	0.00	0.08	0.01	0.05	0.02	99.83				0.888	0.001	1.000	0.001	0.000
std dev	0.27	0.51	0.01	0.04	0.02	0.07	0.02									

Appendix B

Location	Slide(s)	Rock Unit	GPS Co-ordinates	
			Easting	Northing
1	08-D, 08-F	Meguma	451411	4945887
2	07-B, 07-N, 07-C	Meguma	449113	4944561
3	06-B, 06-D, 06-I,	Meguma	447876	4943854
4	05-I	Meguma	447302	4943766
5	05-C, 05-D	Meguma	446948	4943942
6	04-A, 04-B, 04-D	SMB	435326	4967274
7	03-A, 03-B, 03-G, 03-H	SMB	435017	4967628
8	02-A, 02-B	SMB	434531	4968335
9	01-A	SMB	430289	4971384